POLITECNICO
MILANO 1863

SCUOLA DI INGEGNERIA INDUSTRIALE
E DELL'INFORMAZIONE

Preliminary design of an optical sensor for on-orbit debris detection and tracking

Tesi di Laurea Magistrale in
Space Engineering - Ingegneria Spaziale

Author: **Riccardo Caporali**

Student ID: 953437
Advisor: Prof. Mauro Massari
Academic Year: 2021-22.

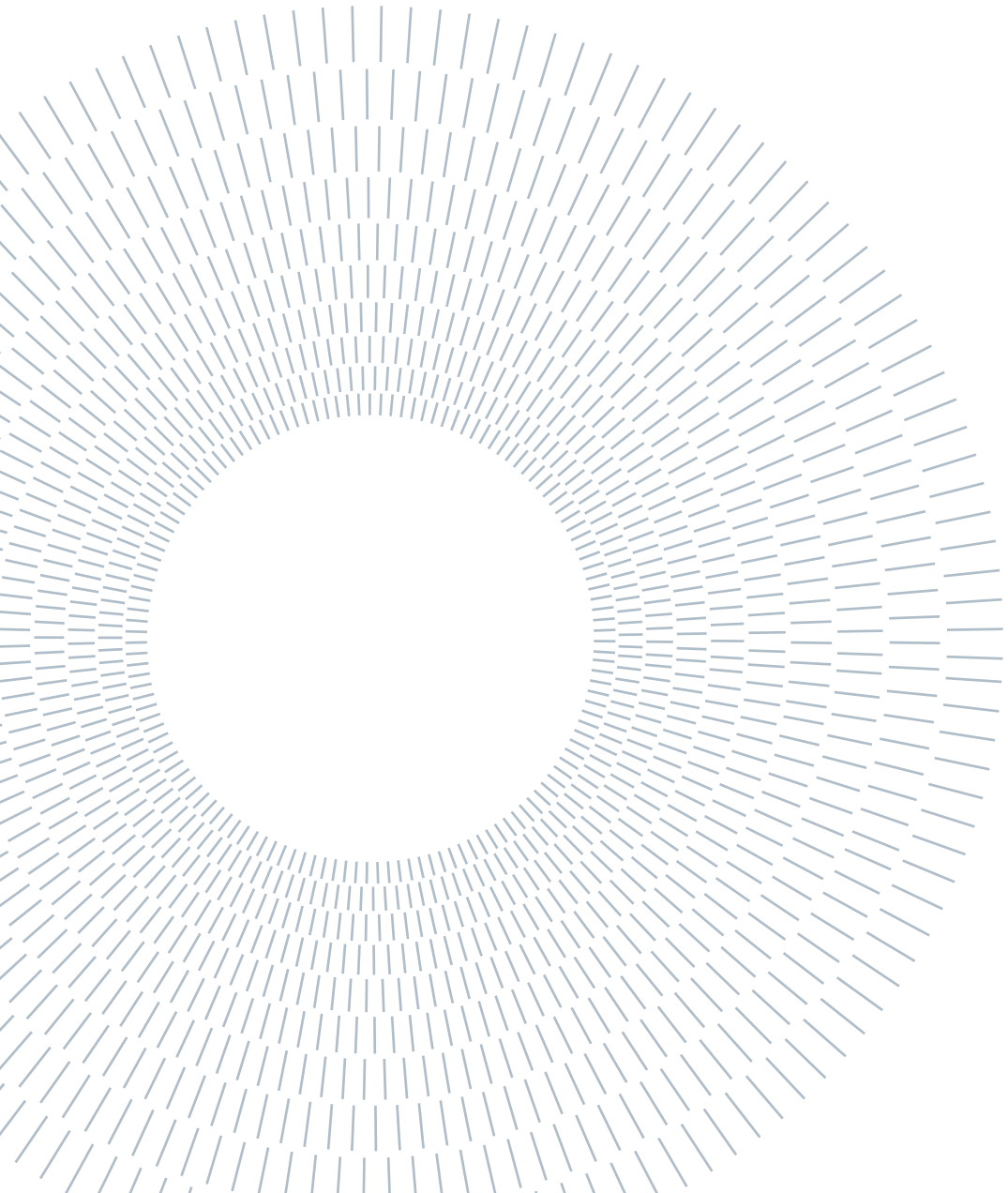

Abstract

The problem of space debris is getting more relevant as time passes. As a matter of fact, the number of object potentially harmful for on orbit satellites is already superior to the hundreds of thousand and it will probably only grow over time. Satellites are normally shielded for space objects with dimensions up to 1 cm, while larger debris are usually tracked by earth-based systems. Anyway are not constantly operating and cannot track all kinds of debris.
The aim of this thesis is the design of an instrument, mountable on satellites, capable of detecting space debris and performing measurements in order to obtain the future trajectory of an approaching object. With the data collected it is possible to estimate if there is any risk of collision between the debris and the satellite.
The design is going to start from zero since no similar instrument have been developed yet. Firstly, the basic functioning of the technology is studied, secondly a trade-off analysis is done in order to select the best instrument architecture. Finally, a more advanced design regarding the instrument components and actual capabilities is performed.

Keywords: Space debris, optical instrument, design.

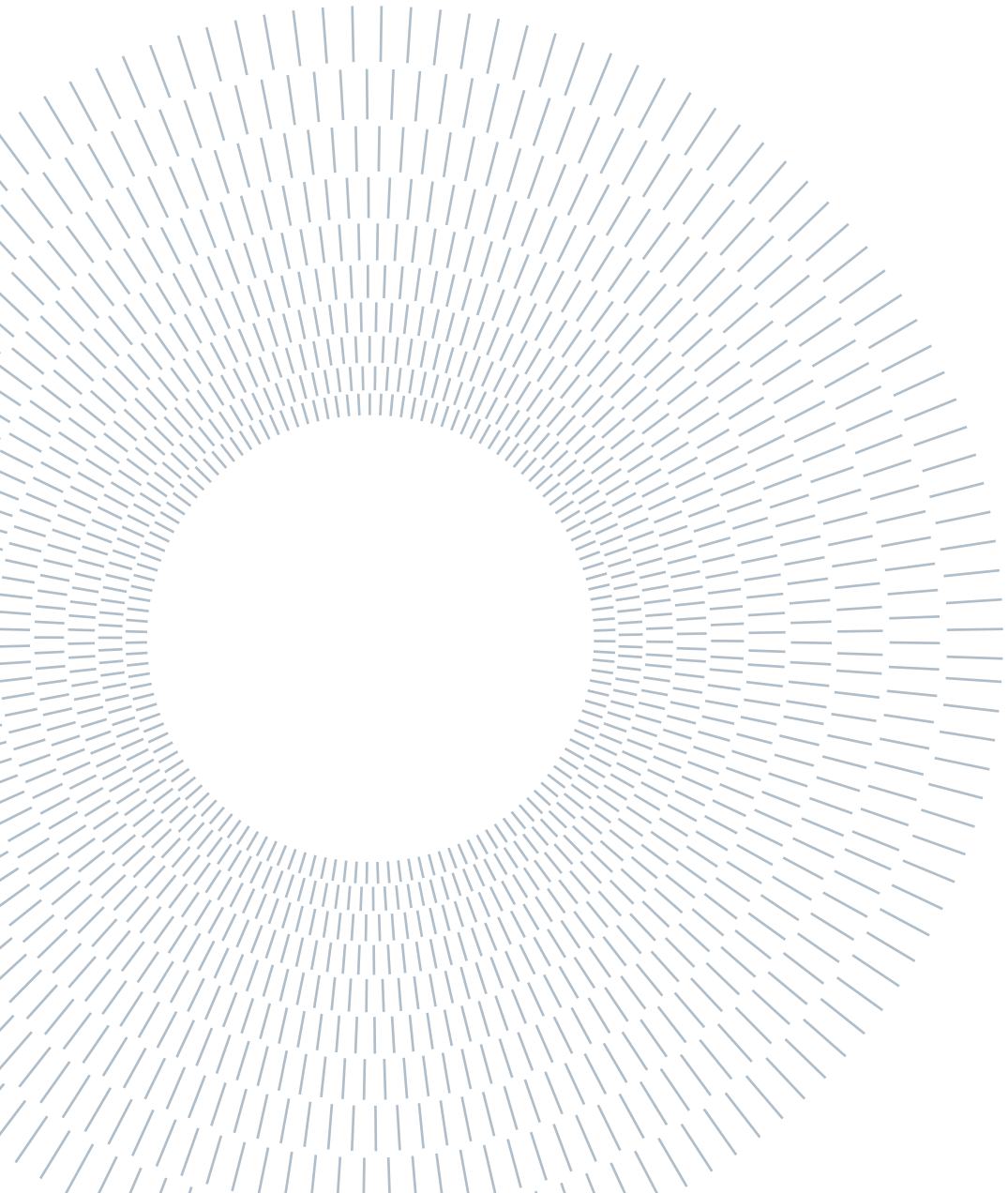

Abstract in lingua italiana

Il problema dei detriti spaziali sta diventando sempre più rilevante, la quantità di oggetti in orbita potenzialmente pericolosi per i satelliti è già superiore alle centinaia di migliaia e probabilmente questo numero continuerà solo che a crescere nel tempo.
I satelliti sono schermati dai detriti con dimensioni fino a 1 cm, mentre i detriti più grandi sono monitorati da sistemi a terra, in ogni caso questi non sono in grado di operare costantemente e tracciare ogni tipo di detrito.
Lo scopo di questa tesi è il design di uno strumento da montare a bordo dei satelliti capace di rilevare i detriti spaziali ed effettuare misurazioni in moda da ottenere la futura traiettoria di questi oggetti; con i dati raccolti sarà poi possibile stimare la possibilità di un eventuale collisione tra il satellite e i detriti.
Poichè non esistono attualmente sistemi simili a quello proposto il design comincerà da zero; per prima cosa verrà studiato il funzionamento di base di questa tecnologia, successivamente un analisi sarà eseguita per la scelta della migliore architettura e configurazione dello strumento, in fine la tesi si concluderà con un design più avanzato dello strumento e delle sue prestazioni.

Parole chiave: Detriti spaziali, strumento ottico, design.

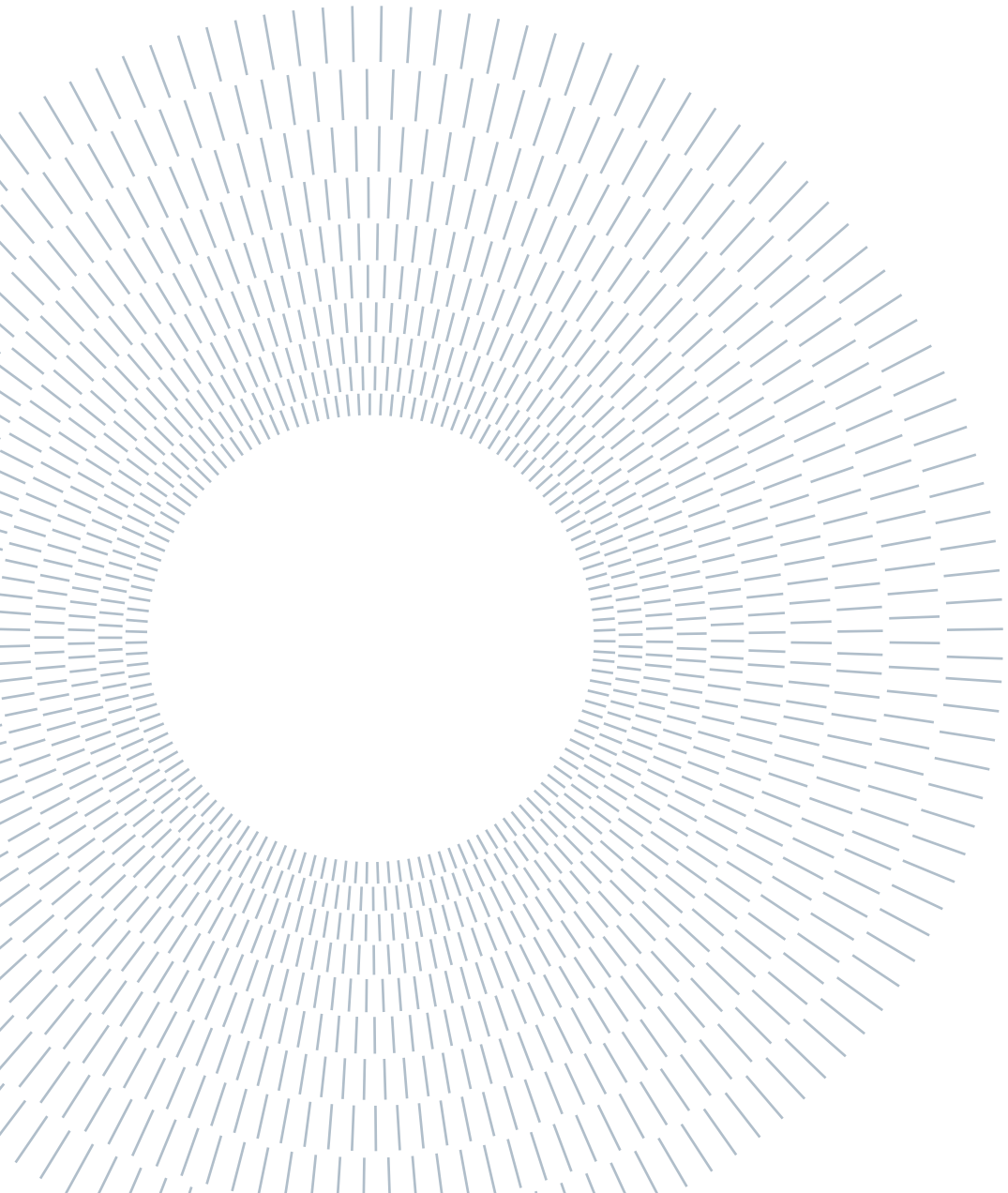

Contents

Introduction

Space debris are human-made objects in space that no longer serve a purpose. These objects include non functioning spacecraft, rocket bodies, mission related debris and fragmentation debris.
The presence of these objects in Earth's orbit create a great problem for the space industry, since even an impact of a satellite with a small fragmentation debris could lead to the destruction of the spacecraft.
The problem of space objects is becoming more and more relevant as time passes. As a matter of fact, the population of space debris in the last decades has been steadily growing and this pattern will continue to be present in the upcoming years. [2].
Currently the space debris problem cannot be solved, in order to reduce the chances of collision with satellites Earth's based tracking systems are utilized. The major issue with these systems are related to the narrow time window for the measurements (sun rise and sun set) and the incapability of detecting small but still harmful debris.
The thesis regards the design of a compact instrument for the detection of space debris to be mounted as a secondary payload into satellites. The instrument would work in close proximity of space debris, mainly detecting objects hazardous for the spacecraft itself and it would be capable of observing an high percentage of objects of all dimensions, even the ones that are not usually seen using ground based sensors.
The first step is to study the space debris environment, achieving a preliminary knowledge regarding the typical dimensions, orbits and composition of space objects. At this point the instrument technology is studied. At first a general analysis on the capabilities and basic functioning is performed. Subsequently, various instrument architectures and configurations are created and the most suitable one is selected. This is done performing a trade-off analysis where each solution is evaluated considering the design drivers of the problem.
The last step is the design of each instrument subsystem (OBDH, optics, PDCU, thermal control) and the final instrument architecture. The thesis is concluded with an analysis on the system capabilities and an estimate on his weight, size and power consumption.

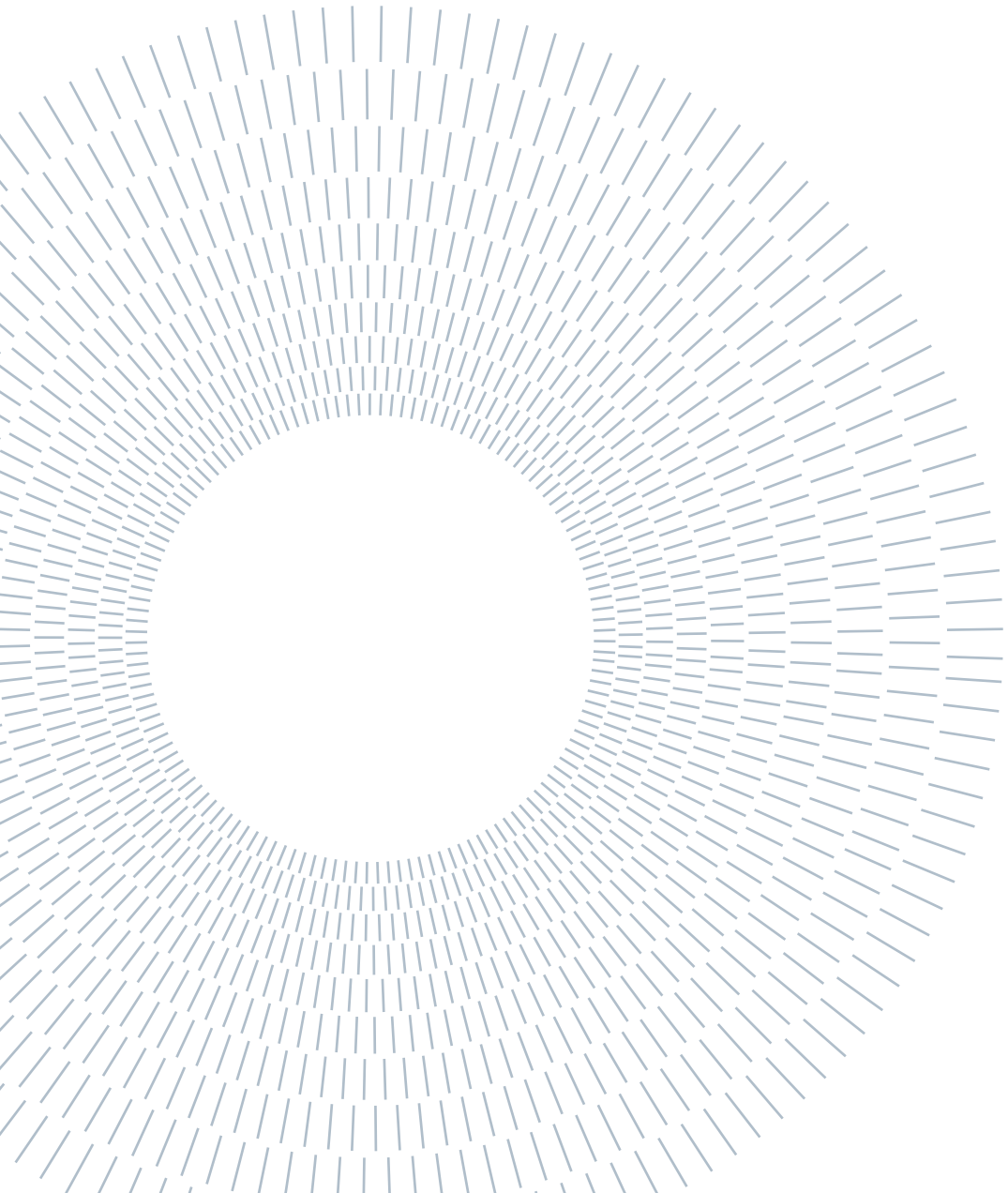

1 | Space Debris Environment

In order to design correctly the instrument, a complete understanding of the problem is needed. For this reason a complete study on the space debris population is reported in this chapter.

1.1. Debris Dimensions

The most effective way of measuring the dimension of the objects is using the diameter (also in most of the cases the object will have a circular shape). Space systems are generally shielded to survive a collision with space debris up to a size of 1 cm. Over that limit, an impact is usually lethal for a space system and this also depend on the relative velocity between the two objects. Collisions with small debris within the critical size range of 1mm to 1 cm may not be harmless to a space system as it can degrade its mission by damaging the payload and other on-board instruments.
Current detection systems are earth based telescopes and radars capable of detecting and tracking debris with a diameter about 5 to 10 cm (or larger) on LEO (Low Earth orbit). It has also to be considered that most of these systems are not always operational (telescopes work properly only during night but the debris need to be illuminated by the sun for example), so debris over 5 cm could represent a threat too.
In LEO it is currently estimated that there are approximately 500,000 of fragments in the middle range (1 cm to 5 cm) in orbit at LEO altitudes. Each of them+ has the potential to cause catastrophic damages to an active satellite. Space debris larger than 1 centimeter has the potential to completely fragment any object it hits. Impacts with larger objects like satellites or rocket body, would add tens of thousands of new space debris fragments to the population.
Debris objects between 3 millimeters and 1 centimeter make up the next category of space debris. An impact will be damaging but it will not necessarily destroy the satellite. These objects cannot be tracked by earth based systems, and it is estimated that there are millions of them in LEO. However, because particles near the lower limit of this category

are so small, they will usually cause only localized damage. Any such damage may still end a satellite mission if the debris hits a critical component such as a computer, sensor, or propellant tank, but the impact will usually not add a significant amount of space debris as it would be the case if the debris fragment was larger.
The last category of space debris comprises objects that are smaller than 3 millimeters, these small particles cause localized damage, particularly in configurations where the surface condition of the impacted spacecraft is important to its function, such as solar arrays and optical systems (telescopes, star trackers, cameras, etc.)[7]. Some spacecraft components can be shielded to prevent damage from debris this size, but not all of them. In the table 1.1 the major characteristics of each size group of debris are reported.

Debris size	**Quantity**	**Impact**	**Track**
$1\,mm$ to $3\,mm$	Milions	Localized damage	Cannot be tracked
$3\,mm$ to $1\,cm$	Milions	Localized damage	Cannot be tracked
$1\,cm$ to $5\,cm$	500000	Major damage	Most cannot be tracked
$5\,cm$ to $10\,cm$	Thousands	Catastrophic damage	Lower limit of tracking
$10\,cm$ or larger	Hundreds/Thousands	Catastrophic damage	Tracked

Table 1.1: **Debris population by size**

The GEO population is largely unknown, the amount of objects is certainly lower but the percentage distribution in dimension should reflect the one from LEO.

1.2. Debris Orbit

The problem related to space debris is highly dependent on the orbit slot that it is considered, specifically two main different environments are present. The first one is the LEO environment, this is the most populated area both in terms of active satellites and space debris. Here, the impacts are the most severe ones due to the high orbital velocities and the occurrence of head-on collisions.
The second one is the HEO (High Earth orbit) environment. In this area the debris population is smaller and mostly concentrated around the GEO orbit. It presents lower orbital velocities and mostly tail-on collisions occur. Anyway, the debris population in this area is largely unknown and tracking usually occurs only for objects with dimensions larger than 1 meter.
In LEO orbits the problem of space debris is much more relevant. This is due to the larger number of both active satellites and unmanned objects present and to the much

higher collision velocities. For this reason, the design of the instrument is going to be more focused on the LEO environment.
In the next part of this section a description of the typical orbital characteristics of the debris population of LEO and GEO is reported. This analysis is essential to understand the environment of the problem and it will be used to model future simulations and design correctly the instrument.

1.2.1. LEO environment

In the LEO environment the problem is the most significant given the number of space debris and high orbital velocities. The debris is not equally distributed in LEO, Its numbers are strictly dependent on the altitude of the orbit [5], as it is shown in Figures 1.1 and 1.2.

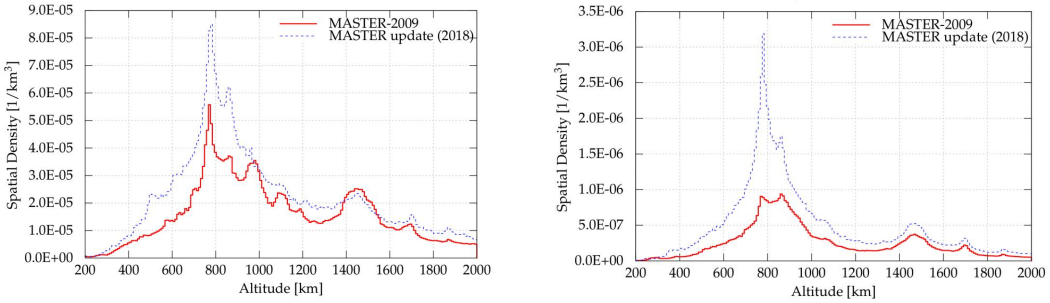

(a) Debris diameter > 1mm. (b) Debris diameter > 1cm.

Figure 1.1: Spatial distribution with spacecraft altitude.

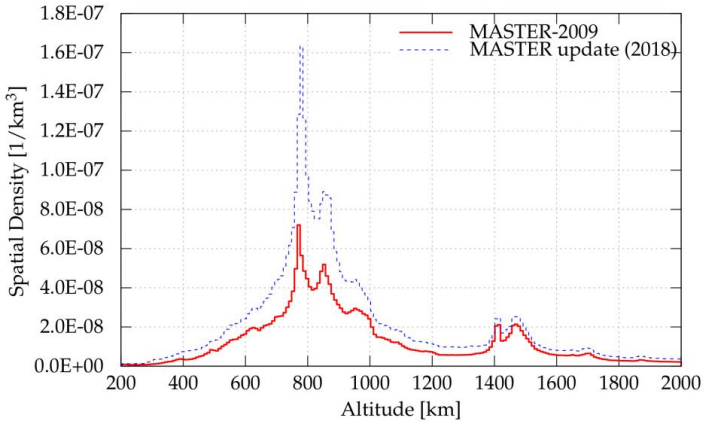

Figure 1.2: Spatial distribution with spacecraft altitude, debris diameter >10 cm.

In general, it would be assumed that for lower orbits it would be easier to track correctly

and catalogue space debris, since the shorter distances make them more easily detectable by Earth based system. In reality the opportunity for repeated observations and the predictability of an object position decreases for orbits with smaller altitudes, making detection and tracking more challenging.
The population of medium-sized (approximately 1 mm to 10 cm in diameter) debris is not nearly as well known as the population of larger debris. To a first approximation, it might be expected that medium-sized debris would be found in about the same orbits as large debris, since most medium-sized debris originates from large objects. However, all large objects may not contribute equally to the medium-sized debris population. Some types of large object (such as rocket bodies that have been a source of explosive fragmentation) may produce much more debris than others. In addition, the perturbing forces affect debris differently depending on its sizes. Medium-sized debris, which often has a higher ratio of cross-sectional-area to mass than large debris, will often be more strongly affected by atmospheric drag and thus, it will experience more rapid orbital decay.
Another important factor to take into account is the characteristics of the orbits, the major parameters to consider are the eccentricity and the inclination; regarding the eccentricity most space debris is placed into circular orbits, this is especially the case for the smaller one (d<10cm).
The inclination of the orbits slightly varies with the debris dimension, in Figure 1.3 the distribution of debris in LEO orbits at various inclination is shown.

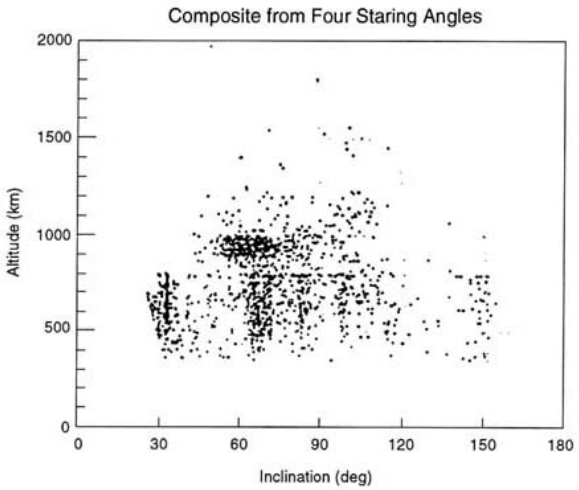

Figure 1.3: Number of debris vs orbital inclination in LEO.

This data is extremely important. Firstly it has to be considered that the possibility of head-on collisions is much higher than tail-on ones. In other words, it is much more likely

for a satellite to impact a debris orbiting in the opposite direction. For these reason, since some orbital inclination are more crowded with space objects, the inclination of the satellites orbit influence greatly the amount of space debris flying by the spacecraft.

1.2.2. HEO environment

The HEO environment is of less interest for the analysis since the main focus of the design is for detection on LEO. Anyway the instrument performances are going to be tested in GEO orbits as well. This is done in order to understand if a possible application of the sensor in that environment could be still useful.
The main focus of this orbital slot is going to be GEO, since the majority of active spacecrafts operate in this orbit. Here satellites maintain actively inclinations close to zero degrees and remain stationary above a given longitude. However, the orbital planes of nonfunctional spacecraft and other debris (due to the Earth's oblateness and third-body gravitational perturbations of the Sun and Moon) constantly oscillate around a plane tilted 7.3 degrees from the equator, causing orbital inclination to vary with an amplitude of 14.6 degrees over a period of about 53 years. In addition, the ellipticity of the Earth's equator will cause debris in GEO to drift away from their initial longitudinal position and oscillate around the nearest stable position (either above 75°E or above 105°W) with a period of more than two years. As a result of these forces, the current population of debris in GEO has a mix of inclinations ranging from 0 to 15 degrees (though fragmentation debris from breakups near GEO may have even higher inclinations) and orbital planes that intersect throughout the entire geostationary ring. [4]
Debris density in GEO has a dependence on longitude as it can be shown in Figure 1.4, this means, that depending on the satellite slot the probability of collision and close fly-by are going to change.

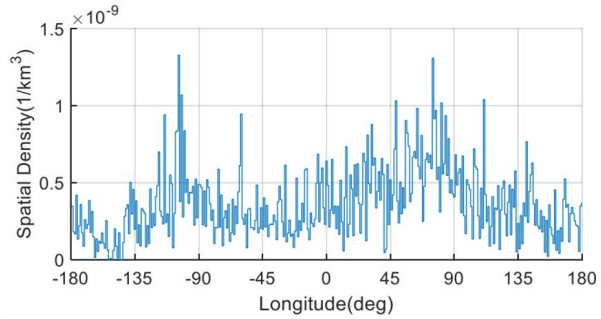

Figure 1.4: Number of debris vs longitude in GEO

1.3. Debris composition

It is important to understand the composition of debris, different surfaces and materials react differently to light or radio waves. For this reason this analysis will greatly influences the design of the instrument. In Figure 1.5 the composition of space objects is reported:

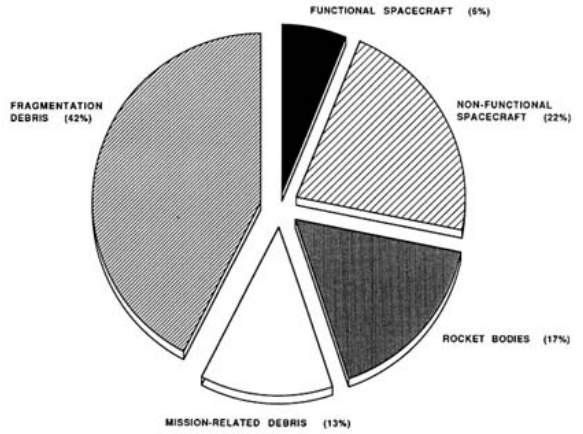

Figure 1.5: Space objects composition

As we can see active spacecrafts represent only a small fraction of space objects in orbit, while the majority of them is composed by fragmentation debris [1]. Fragmentation debris has a wide variety of dimensions spacing from millimeters or smaller up to 10 centimeters and their composition is reported in the Graph 1.6.

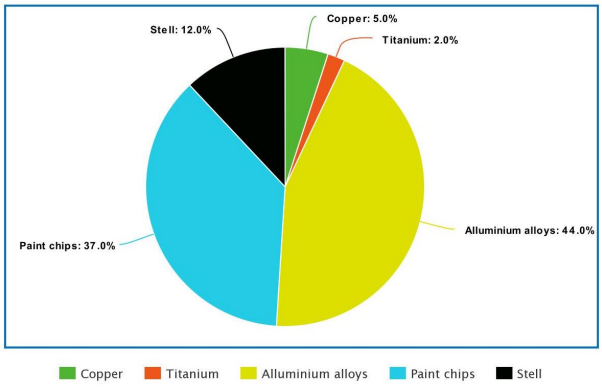

Figure 1.6: Fragmentation debris composition

This study is going to be useful during the design phase since it will help derive the debris optical characteristics.

2 | Optical instrument

2.1. Introduction

The detection of space debris using optical system can be done by detecting the reflected sunlight coming from the debris or by detecting the emission of the object in the Far infrared range(FIR).

In order to obtain the detection of the debris, the incident light coming must be enough to produce a signal with a high enough SNR (Signal to noise ratio). This depends on various factors some o which are related to the instrument (aperture area, number of pixel,ecc) and some other to the problem conditions (debris distance,reflectivity of the surface,ecc). In the following analysis is shown how all these characteristics influence the final performances of the instrument and the theoretical values achievable using this technology.

2.2. Signal contribution

The base of the design is to find the relation between the Signal to noise ratio, the problem variables and the instrument characteristics.
The SNR is the relation between the signal and the noises contribution, it can be computed as shown in Equation.2.1.

$$SNR = \frac{e_s}{\sqrt{(e_s + e_b + e_d + e_n^2)}} \tag{2.1}$$

In the equation e_s is the contribution of the signal coming from the target and it is expressed in $electrons/pixel$. e_b, e_d and e_n are the noises contributions respectively from: backgroung, dark current and readout, expressed in $electrons/pixel$.
As said in the introduction the two possible solutions that are considered are the measurement of the reflected sun light coming from the space debris or the detection of the

emitted radiation on the FIR wavelengths.
While the computation of the noise contributions in the two cases is the same (only few value changes), the procedure to obtain the signal photoelectrons e_s is different in the two cases. Regarding the measurement of the reflected radiation, the procedure to obtain the signal is reported in Section 2.3 while for the emission measurement case in Section 2.4.

2.3. Detection of the reflected radiation

The system in this case is a passive instrument, so it relays in an external source of light in order to function properly. The light emitted by the sun gets reflected by the debris, travels a certain distance and enters the instrument optical system. The photons hit the detectors pixel and a flow of electrons (e_s) proportional to the amount of photons is generated inside each pixel.

Firstly, it is needed to understand the debris optical signatures in order to estimate the efficacy of passive sensing approaches. These signatures can be expressed by the debris visual magnitude and they are based to first order on the debris size and optical properties. The unit less and logarithmic magnitude system references the star of Vega as a zero point, resulting in the sun having a visual magnitude (m_{sun}) of -26.73. The signature of an object (m_{obj}), when approximated as a sphere, and illuminated by the sun is reported in Equation 2.2.

$$m_{obj} = m_{sun} - 2.5log\left[\frac{d^2}{R^2} \cdot \rho \cdot P(\psi)\right] \tag{2.2}$$

Where d is the diameter of the object, R is the distance between the object and the observer, is the reflectance, and p() is the solar phase angle function. The solar phase angle is the angular extent between the sun and the observer, relative to the object, for the analysis a value of 90 deg is selected. For diffuse, or Lambertian, surfaces, the total reflected energy decreases with increasing phase angles, while for specular or mirrored surfaces, there is no such dependency.
Our estimates assume equal contributions from both specular and diffuse reflectance components, which is supported by observational data. Gray body reflectance will be considered for the objects, such that is constant for all wavelengths. For a sphere, the specular phase angle function is a constant $\frac{1}{4}$, while the diffuse P_{diff} phase angle function is given by Equation 2.3. [6]

$$P_{diff}(\psi) = \frac{2}{3\pi} \cdot [sin(\psi) + (\pi - \psi) \cdot cos(\psi)] \tag{2.3}$$

The signature of a spherical object using both specular and diffuse components is reported in Equation 2.4.

$$m_{obj} = m_{sun} - 2.5log\left[\frac{d^2}{R^2} \cdot \left(\frac{\rho_{spec}}{4} + \rho_{diff} \cdot P_{diff}(\psi)\right)\right] \tag{2.4}$$

Regarding the reflectance, the specular (ρ_{spec}) and diffusive (ρ_{diff}) component are considered equal, the value of this parameter depends on the debris surface optical properties, for this first analysis the most common value of 0.2 for this parameter is considered;[3] this is in general the reflectivity coefficient of rocket bodies, inactive satellite and most of the metallic fragments.

The first step to compute the signal contribution is the conversion of visual magnitude of the debris (m_{obj}) to photon-based irradiance. This is accomplished by converting the zero magnitude power flux density into photon density via multiplication by (λ / h c) where h is Planck's constant, c is the speed of light and λ is the wavelength.
The resulting photon irradiance (E_{deb}) as a function of visual magnitude is shown in Equation.2.5.

$$E_{deb} = \frac{\lambda \cdot 10^{-0.4mobj}}{h \cdot c}[ph/s/m^2] \tag{2.5}$$

Solar-reflected light from a debris object is first transmitted with an irradiance of E_{deb} to an optical system having an aperture area of A.
Upon reaching the aperture, losses are incurred before arriving at the detector due to the finite optical transmittance (τ) of the optics. Once incident upon the detector, the photons are converted to signal photoelectrons (e_s) according to the solar-weighted quantum efficiency (Q_E) of the detector.
Finally, the signal photoelectron rate obtained is multiplied by the signal evaluation time (t_{eva}) to make the conversion to the total number of photoelectrons. The number of signal photoelectrons (e_s) is therefore given by Equation-2.6

$$e_s = Q_E \cdot \tau \cdot A \cdot E_{deb} \cdot t_{eva} \tag{2.6}$$

Regarding the signal evaluation time t_{eva}, this is computed considering the minimum time a debris would stay inside a single pixel as the worst case scenario. The debris will move relatively to the instrument and after a certain amount of time the light will go from one pixel to the adjacent one, the length of this time depends on the Field of view (FOV) of the instrument, the relative angular velocity of the debris with respect to the instrument (w) and the number of pixel of the detector (n_{pixel}). The formula is shown on Equation.2.7.

$$t_{eva} = \frac{FOV}{n_{pixel} \cdot w} \tag{2.7}$$

It is important to underline the fact that this is not the actual integration time of the detector, but only the time that the debris reflection will stay inside a single pixel before passing to the adjacent one.
Debris having high angular velocity, during the integration time will pass through multiple pixels, subsequently the final image will not see a single pixel illuminated by the debris but a line spamming through multiple pixels.

2.4. Detection of the emitted radiation

In the previous section the computation of the signal generated from the reflected radiation from a debris was shown. Hereafter the same study for the radiation emitted from an object is presented. The emission of a body in the infrared region is strictly dependent on the temperature of the object and thus also the signal photoelectrons (e_s) are going to depend on the debris temperature as shown in Equation 2.8.

$$e_s\left(T\right) = \frac{d^2 \cdot A \cdot \tau \cdot t_{eva}}{2 \cdot \pi \cdot h^2} \int_{\lambda_1}^{\lambda_2} Q_E \cdot \frac{L(\lambda, T)}{E_p(\lambda)}\, dx \tag{2.8}$$

Where A, d, τ and Q_E are the same variables defined in the section before, $L(\lambda, T)$ represents the black body spectrum given by the Planck's law. $E_p(\lambda)$ is the energy of a photon at wavelength λ. The integral is performed between the bounds of the two bands of 11.5 [μm] and 15.5 [μm]. The body temperature is set to 273 K for this first general analysis. Finally t_{eva} is the evaluation time and it can be computed as shown in the section before.

2.5. Noise contribution

In total there are three sources of noise considered in this analysis as reported in subsection 2.1: background noise, dark current and read noise. As for the signal contribution, the aim of this analysis is to compute the amount of photoelectrons generated from each noise source.

Background noise, is the noise generated due to photons coming from the background of the image that enter the detectors and generate an unwanted signal. In order to estimate the value of this noise it is essential to start with the optical signature of the background. As with debris optical signatures, this background radiance specification must be converted to absolute radiometric units. Given a background of Mb in units of visual magnitudes per square arc second (L_b), the conversion to absolute radiometric units of photons per second per meter squared per steradian is shown in Equation 2.9.

$$L_b = 5.6 \cdot 10^{10} \cdot 10^{-0.4Mb} \cdot \left(\frac{180}{\pi}\right)^2 \cdot 3600^2 \left[\frac{ph}{sec \cdot m^2 \cdot sr}\right] \tag{2.9}$$

Usually the background would be deep space, its magnitude can vary from 18 to 22, for this analysis the highest possible values of 18 is selected since it represents the worst case scenario.
As for the photons coming from the debris, the light from the background enters the system, passes through optics with a certain optical transmittance (τ) and it gets converted into electrons by the detector having a certain quantum efficiency QE. The noise contribution in photoelectrons can be computed as reported in Equation2.10.

$$e_b = \frac{L_b \cdot S_a \cdot \tau \cdot QE \cdot t_{int} \cdot A}{n_{pixel}^2}. \tag{2.10}$$

A is the optic aperture area, S_{angle} is the solid angle created by the system FOV and n_{pixel} is the number of pixel (per row) of the detector. Regarding t_{int}, this is the integration time of the detector, the amount of time the sensor measure the signal before resetting. While the debris is staying inside a pixel for a far less amount of time (considering the worst case), the background light is going to reach all the pixels contemporaneously and get converted to photoelectrons for all the integration time of the detector.

Read noise, is the amount of noise generated by electronics as the charge present in the

pixels is transferred. It is a combination of all the noise generated by system components which convert the charge of each CCD pixel into a signal for conversion into a digital unit. The value of this noise varies depending on the detector in use; since at this stage of the design there is not a detector selected yet, this contribution is set to 20 $[e^-/pixel]$.

Dark current is the electric current that flows through photosensitive devices such as a photomultiplier tube, photodiode, or charge-coupled device even when no photons enter the device. This noise consists of the charges generated in the detector when no outside radiation is entering the system. This noise component is strictly dependent on the temperature of the detector and it can be computed as reported in Equation 2.11.

$$e_d = \frac{1.5 \cdot S_d \cdot A_{px} \cdot G \cdot t_{int}}{q}. \tag{2.11}$$

Where A_{px} is the area of a pixel, G is a gain, q is the charge of an electron. S_d is a variable depending on the detector temperature and it is computed by the sum of two contributions as shown in Equation 2.12.

$$S_d = \alpha \cdot S_s + S_b \tag{2.12}$$

$$S_s = \frac{122 \cdot T_{det}^3 \cdot e^{-6400}}{T_{det}} \;\; ; \;\; S_b = \frac{3.3 \cdot 10^{-6} \cdot T_{det}^2 \cdot e^{-9080}}{T_{det}} \tag{2.13}$$

Where α is the electron to count conversion efficiency and T_det is the temperature of the detector in Kelvin.

3 | General optical system capabilities analysis

In this chapter a general overview of the instrument capabilities and basic equation is presented.
As a start to the analysis the minimum SNR threshold for detection in set to an appropriate value of 14 Db. The procedure then consist in solving the equations of the previous chapters in opposite to compute the range of the instrument.
The analysis is done considering various debris sizes changing from 1mm to 1 m and for different optics geometries.
As a first step it is important to select the correct wavelengths for the measurements, regarding the detection of the reflected radiation. The possible wavelengths are the visible or Near infrared (NIR), where the sun emission is high enough. Regarding the detection of the emitted radiation, the wavelength is the Far infrared one, since bodies usually emit in this range. The comparison between the three possible solutions is shown in Figure 3.1.

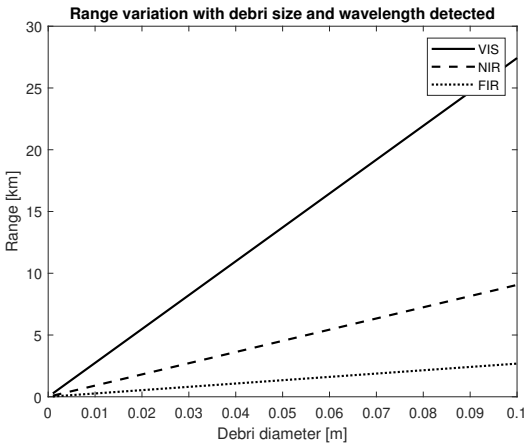

Figure 3.1: Range capabilities visible vs NIR vs FIR

Between the visible and NIR configurations the only difference is the detector, since the first solution presents much higher range capabilities, the instrument will not work in the

NIR region. Regarding the FIR wavelength, it presents very low performances but it has the advantage of working during Earth's shadow since it detects the emitted radiation but not the reflected one.
This solution is not going to be selected as the main one due to the much lower capabilities but it will be analyzed in further parts of the design.

Hereinafter the analysis shifts into understanding the basic relations between the various instrument parameters (aperture diameter, FOV, F number) and the instrument performance. This is going to be only a preliminary analysis to obtain a better understanding of the problem, in the next chapter the actual design of possible instrument and trade-off analysis are going to be performed.
Now considering the aperture diameter of the instrument, it is related to the instrument Range as reported in Figure 3.2.

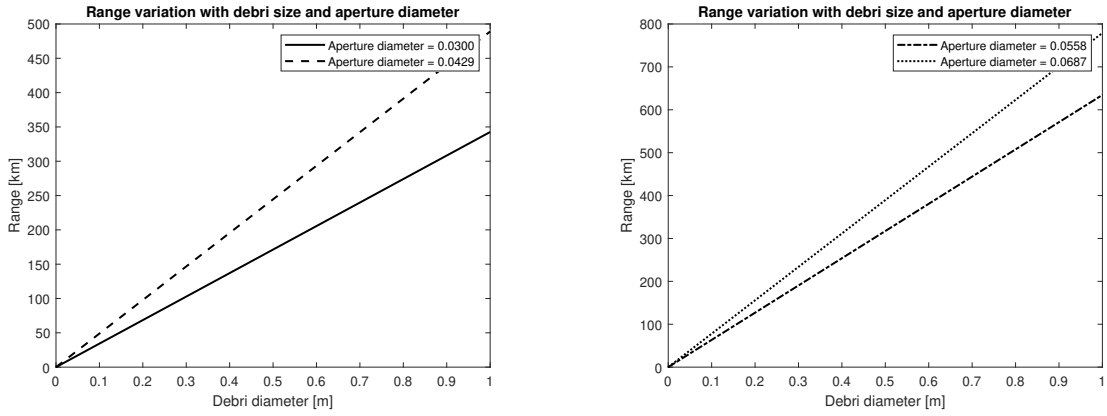

(a) VST-41M architecture

(b) ST-400 architecture

Figure 3.2: Range variation with debris size and aperture diameter

As we can see the range capabilities highly increase with the aperture diameter, in the next phase of the design this is going to be one of the main parameters changing between the proposed architectures.

Other important parameters of the instrument are the FOV and F number and are strictly related to each other, they can be computed as shown in Equation 3.1.

$$FOV = \frac{360}{\pi} \cdot \tan^{-1}\left(\frac{d_s}{2 \cdot f}\right) \;\; ; \;\; F = \frac{f}{D} \tag{3.1}$$

Where f is the focal length of the instrument, d_s is the detector size and D is the aperture diameter. As reported in Figure 3.3, in order to have high FOV for the instrument, a low F number is required (this particular graph was done with reasonable values for the aperture diameter and detector size).

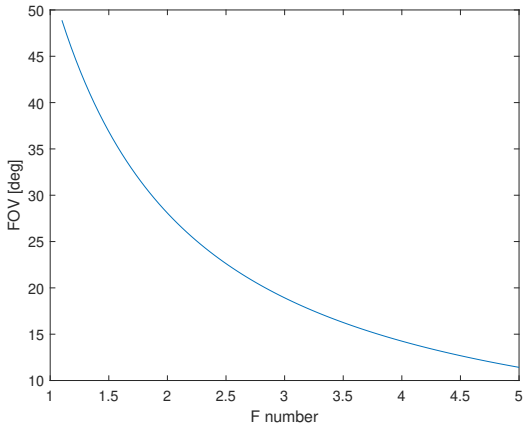

Figure 3.3: FOV and F number relation

Another important factor to be considered in this analysis is the resolution of the instrument. This variable is going to be of great interest in future trade-offs. There are two main components influencing the resolution limit of the instrument. The first one is the Instantaneous Field of View, an angle that representing the portion of FOV seen by a singular pixel, it can be computed as shown in Equation 3.2. The second component is the resolution limit given by diffraction phenomena and it is defined as the bending of waves around the corners of an obstacle or through an aperture. It can be computed as reported in Equation 3.2.

$$IFOV = \frac{FOV}{n_{pixels}} \;\; ; \;\; r_{diff} = \frac{1.22 \cdot \lambda \cdot 180}{D \cdot \pi} \tag{3.2}$$

The variable n_{pixels} is the number of pixels (per row) of the instrument, λ is the light wavelength and D is the aperture diameter. The variation of the two contributions with the aperture diameter is reported in Figure 3.4.

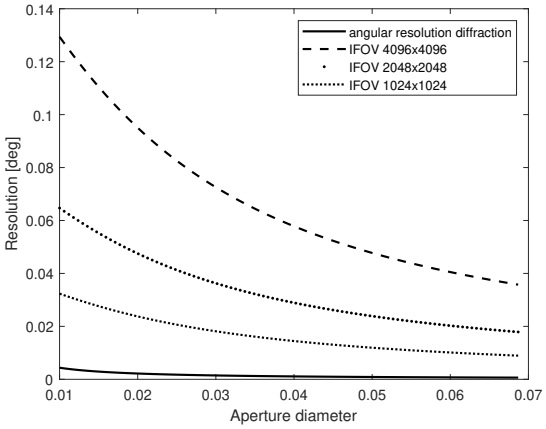

Figure 3.4: IFOV and diffraction aberration with aperture diameter

The contribution of the diffraction can be neglected in a first preliminary analysis since it has much smaller impact with respect to the limitations given by the IFOV.

4 | Optical instrument trade-off analysis

In the previous chapter the general capabilities of the instrument were shown, now a more advanced phase of the design is initiated.
Firstly, the design drivers are chosen. Subsequently a trade-off between multiple possible solutions created from the baselines is performed. The different architectures are evaluated based on the design drivers and the best ones are selected for further design. Finally, a last trade-off regarding the general configuration and number of sensors is performed. This study marks the end of the preliminary phase of the design, a single best solution will be selected for the final phase of the design.
The instrument design and trade-off analysis are going to be performed considering the LEO environment as the main one for the operations of the instrument. This does not mean that the instrument cannot be operated on board spacecraft placed in different orbits, as for example GEO ones, but that is going to be optimized for the operations in LEO.
This choice is done considering that in the LEO environment the space debris problem is the most relevant one, more satellites are operating here, the debris population is much bigger and there is more difficulty to track with Earth-based sensors.

4.1. Design drivers

The design drivers are selected in order to specify the most important instrument parameters and subsequently their optimization is essential to achieve the optimal design.
Here below the main design drivers for the optical system are reported:

Detectable magnitude, this driver represents the capability of the instrument to detect and measure a source of light. The visual magnitude is a brightness measurement unit. This parameter depends strictly on the instrument characteristics and the environment

of the problem. Moreover, it is independent on the distance and size of the target.
For example, if the instrument is capable to detect visual magnitudes up to 14 this mean it would be capable to see debris of 10 cm at a distance of 50 km and debris of 1 meter at 150 km. This parameter is essential for the design since higher visual magnitudes detectable leads to increase the capability to see farther and smaller debris in general, making it detect a higher amount of objects.

Resolution, it influences the accuracy related to the debris trajectory reconstruction. Higher accuracy leads to less ambiguity on the target position.
As seen in the previous chapter the resolution is dependent of the FOV of the instrument, the number of pixels and the aperture diameter.

Detection ratio, this driver is expressing the percentage of space debris detected by the instrument out of the total amount passing close to the satellite.
For example if the number of debris passing close to the satellite is 100 in one orbital revolution and the instrument is capable of detecting only 60 of them, the detection ratio is 60/100.
A debris is considered dangerous if it passes in proximity of the satellite, this mean that the orbit of the two could potentially have a point of intersection and an impact may occur in the future. This is much more rare with a space object that has not passed close-by to the satellite in previous orbits.

Mass, this is obviously an important factor in order to reduce the launch cost brightness measurement unit. Additionally, it is important to underline the fact that the instrument in analysis will not be the main payload of the spacecraft. Tts presence must affect as little as possible the spacecraft maneuverability and the main payload operations.

Size, as for the mass it has to be limited as much as possible in order to let the instrument fit more easily inside the spacecraft and cause less encumbrance.
The size of the instrument will be greatly influenced not only by the optical system dimensions, but also from other instrument components like the detector, possible cooling system, computer and electronics.

Power, has to be limited as possible and it depends mostly on the energy consumption of the detector and if present the cooling system. This will be influenced by the data

processing of the signal, heavier measurements and computation will usually increase the power needed by the instrument computer.

4.2. Instrument architecture trade-off analysis

4.2.1. Introduction

This trade-off analysis compares different instrument architecture and characteristics. Each solution is evaluated on how it performs in regards of the design drivers.
For each of them the advantages and disadvantages are going to be highlighted and finally the best solutions are going to be chosen for the next phases of the design. It is going to be shown that this analysis will not highlight a single solution as the best one. In fact, the study will highlight two architectures as the most suitable ones.Only in the last trade-off, where the configuration of the instrument is considered, the actual best architecture is going to be selected.

For this first trade-off three different instrument architectures are analyzed, the main parameters changed between the configuration are: detector size, number of pixel,FOV and aperture diameter. These values are not taken casually but they are based on the dimensions of a certain star sensor. This is done in order to easily establish mass, size and power of each architecture. The approximation is reasonable since the instruments are similar to each others and the way these characteristics change between an architecture and another resemble the one of the star sensor. Regarding the analysis the resolution and detectable magnitude capabilities are computed using the expressions reported in chapter 2.

4.2.2. Matlab Simulation

In order to compute the detection ratio of each configuration, a Matlab simulation is utilized. The satellite is placed in a circular LEO orbit, while 6000 debris are placed in similar circular orbits. The dimensions of the debris space between 5 cm to 10 m, following the percentage distribution presented in Section 1.1.
The inclinations of those orbits are selected using studies presented in the previous chapter.
The semi major axis of the debris orbits are generated randomly, having a mean value equal to the satellites orbit semi major axis and a standard deviation of 15 km. The other orbital parameters are random since they don't influence the analysis.

The orbits of satellite and debris are then propagated and at each time step of 10 s two main things are computed: if the debris are close enough in order to be seen by the instrument and if they are inside the FOV of the sensor. If both of these conditions are verified the debris is detected by the sensor and the data is saved. The simulation consider the instrument pointed towards the direction of motion of the satellite and the time span of the analysis is 10 days. It is being taken into account the impossibility of detecting debris during the time the satellite is in the Earths shadow.
The parameters selected randomly are the true anomaly, right ascension of the ascending node and the anomaly of the perigee, for both the satellite and the debris. In order to have the results of the simulation independent from their value, the analysis is repeated a great number of time, having these variables changing randomly in every run, at the end the mean results of all the simulations are computed.

4.2.3. Instrument architecture data

In this section the characteristics of the instrument architectures tested are reported. As said before the instruments are designed starting from 3 different star sensors as baseline. Between the configurations the only parameters changing are: FOV, number of pixels of the detector, aperture diameter and detector dimensions.
The first architecture is based of the Star tracker "VST-41M", the second one from the "ST-400" and the third one from "ST-200". The systems data are reported in Table 4.1.

	VST-41M	**ST-400**	**ST-200**
FOV	30	40	40
# of pixels(x row)	4096	4096	2048
Aperture diameter [m]	0.07	0.05	0.02
Detector dimensions[m]	0.04	0.04	0.015
Mass [g]	700-900	250-350	50-100
Size [mm]	100x100x120	50x50x60	30x30x40
Power	1.5	1.5	1
Resolution [deg]	0.0073	0.0098	0.0195
Detectable magnitude	5.64	5.13	3.62
Detection ratio [%]	39	33	16

Table 4.1: Highlighting the columns

The first and the second instrument present similar architectures, both of them use the same detector but they have different optical systems. The first one has a higher aperture diameter that greatly increase the detectable magnitudes of the instrument but at the same time limit the FOV. The limitations of this parameter increase the resolution capabilities of the instrument and the main drawback is the higher mass and size.
The last configuration is a more compact one, this greatly limits the performances but reduces mass, power and size requirements.
The third configuration shows much lower performances with respect to the others and it's not considered in further analysis. The first configuration has the best performances but not much higher considering the second one, that in the other hand is much more compact. For this reasons both the first and the second architectures are analysed in the next trade-off where more types of system configurations are tested.

4.3. Instrument Configuration trade-off analysis

In the previous analysis we have selected the instruments architecture having the best characteristics, now various configuration will be tested and the one showing better results in regards of the design drivers will be selected.
Since the instrument is the same in all of the configuration parameters like the resolution and the detectable magnitude will not change. The main trade-off will be between the detection ratio and power,mass,size of the instrument, that are closely dependent on the number of sensor of a configuration.
In total ten configuration are proposed and they are different in terms of number of instrument and pointing direction. A particular configuration is made to study the possibility of adding a detector capable of measuring radiation emitted from the debris in the FIR wavelengths.
Here below the list and basic functioning of the configuration is presented:

One instrument dom, a single instrument pointing in the direction of motion (dom), this configuration can spot more easily debris in orthogonal orbits with respect to the one of the satellite (inclination difference around 90°).

One instruments opposite of dom, a single instrument pointing in the opposite of the direction of motion, also this configuration can spot more easily the kind of debris of the previous configuration. as a result, small differences in performance with the previous architectures are expected.

Two instrument, one in dom and one opposite, this configuration gives better result with respect to the two previous analyzed given the fact that two sensors are being used. The major drawback is the increment in mass, size and power requirements of the instrument.
Anyway, the architecture gives higher results in terms of number of debris (out of the total) detected since it sees double the amount of objects orbiting orthogonal to the orbit of the satellite. While more or less the same amount of debris having small or high inclination differences (close to 0° or 180°) are detected.

Two instruments in dom, this configuration is the equivalent of having an instrument with double the FOV. In this case the debris detected consecutively are the ones with medium inclination difference (around 90°) and they detect a greater amount of debris with small or high inclination difference.

One instrument orthogonal to orbital plane, this configuration is analyzed in order to directly compare it with the first two. This solution should be more capable of detecting debris orbiting with small or high inclination differences.
Theoretically, better performances are expected with respect to the first two configurations since debris with high inclinations difference perform fly-by with the satellite more frequently.

Two instruments in dom, in practice this is a single instrument having two detectors, one thermal and one visible pointing in the same direction.
The major advantage of this configuration is the capability to detect debris in earths shadow thanks to the thermal detector sensible to radiation in the FIR range.
Anyway, the range capability of this component are much lower since the light component emitted from the debris is only a fraction of the reflected one.
This architecture is not as damaging for size and mass as the ones relaying in two instruments since in this case the thermal and visible detector share the same optical system. A higher weight and size is given just by the diffraction grid and thermal detector.

Two instruments, one in dom and one orthogonal, here the sensors detection is more complete being capable of detecting equally different kinds of debris.

Three instruments 1, here the configuration is composed by 3 sensors, one in dom, one opposite and one orthogonal. This clearly leads to better result with respect to the previous configurations but at the cost of higher mass, size and power requirements.

Three instruments 2 ,the configuration is composed by 3 sensors, one in dom, one orthogonal and one opposite. This solution is equal to the previous one but the only difference is the pointing direction of the sensors. It will be shown that the analysis of these two configurations lead to very similar results.

Four instruments, the four sensor are pointed in the following manner; one in dom, one opposite to dom, one orthogonal and one opposite to orthogonal. These clearly lead to the best results in terms of debris detected but at the cost of much higher mass, size and power requirements.

The conditions of the analysis are the same of the previous trade-off. As stated before the solutions are analyzed for both architectures based respectively on the $VST-41M$ and $ST-400$ star sensors. In Figure 4.1a and 4.1b are reported the results for the first and second architecture.

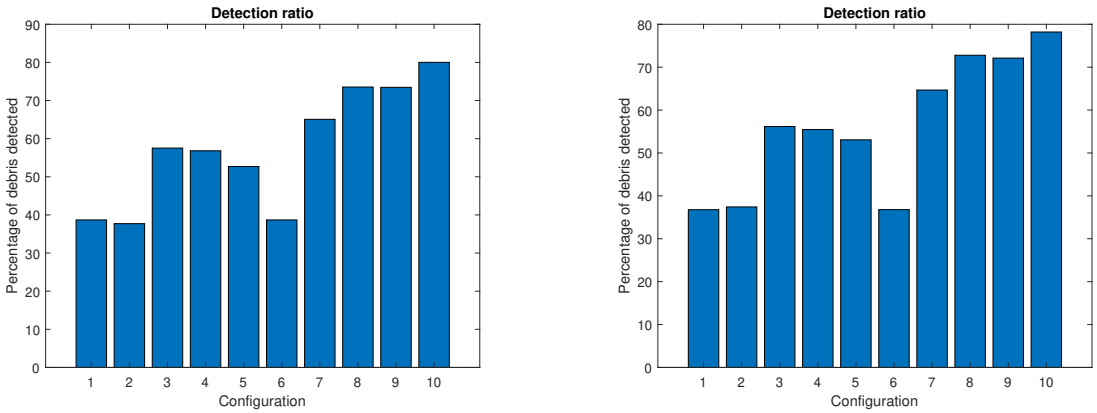

(a) VST-41M architecture (b) ST-400 architecture

Figure 4.1: Detection ratio with instrument configuration

As a first step the two instrument architectures are going to be compared. It is clear that the first instrument architecture has higher performances and as it was underlined in the section before, it also has slightly higher resolution. Anyway the $ST-400$ architecture

shows much less mass and size requirements.
In the configurations with multiple instruments the differences in detectable magnitude are much less relevant while the importance of the mass and size constraints are crucial. For this reason the architecture selected is the one based on the star sensor $ST-400$.

Regarding the analysis on the instrument and the trade-off between the various configurations.
Firstly, similar solutions having the same amount of sensors are confronted with each others. As a result, the best one for each group will be selected and finally the best between all will be chosen.
This first trade-off is fairly easy, here instrument with similar mass, size and power are compared and the only driver changing is the detection ratio. After this analysis the remaining best 4 instruments for each category will be compared also considering other design drivers.

One sensor: Regarding the configuration with one sensor, the trade-off is simple since under every characteristic these solutions are equal except for the detection rate. Each configuration is composed by one instrument and the only difference is the pointing direction. The best solution (between 1,2,5,6) is the sensor pointing orthogonal to the direction of motion (5) as it can be seen in table 4.2.

	1	**2**	**5**	**6**
Detection ratio [%]	36.7	37.4	53.1	37.8

Table 4.2: Detection ratio one sensor configuration

This result is independent from the satellites specific orbit since the analysis has been carried out for a generic LEO circular orbit with inclinations varying for each repetition of the simulation. The configuration 6 is considered here since the thermal and optical sensors are considered part of the same instrument, it is compared to the first configuration since it has the same pointing direction and it is clear that the small increase in performances is not worth the higher mass and complexity of the system.

Two sensors: The configurations having two sensors are (3,4,7); similarly to the previous case the best performances is obtained by the configuration having one instrument

pointing in the orthogonal direction(7).
The result of detection ratio for each configuration is shown in Table 4.3.

	3	**4**	**7**
Detection ratio [%]	56.1	55.5	64.8

Table 4.3: Detection ratio two sensors configuration

As predicted at the start of the section, the sensors pointing in the orthogonal direction are more capable of detecting debris orbiting with high inclination difference, the ones that more often perform fly-by with the satellite.

Three sensors: Here the choice is between the configuration 8,9. They show similar results (around 72 %) and they are to be considered equal, the difference in the architecture is just the pointing direction and depending on the specific orbit of the satellite one could perform better than the other.

For the final trade-off the four configurations are going to be analyzed considering also the other design drivers.

- One sensor orthogonal to the dom (configuration 5)
- Two instruments, one in dom and one orthogonal (configuration 7)
- Three instruments (configuration 8)
- Four instruments (configuration 10)

The resolution and detectable magnitude are not being considered since the architectures share the same instrument.
Another important aspect to be considered at this point of the analysis is the detection ratio for different debris dimensions reported in Figure 4.2.

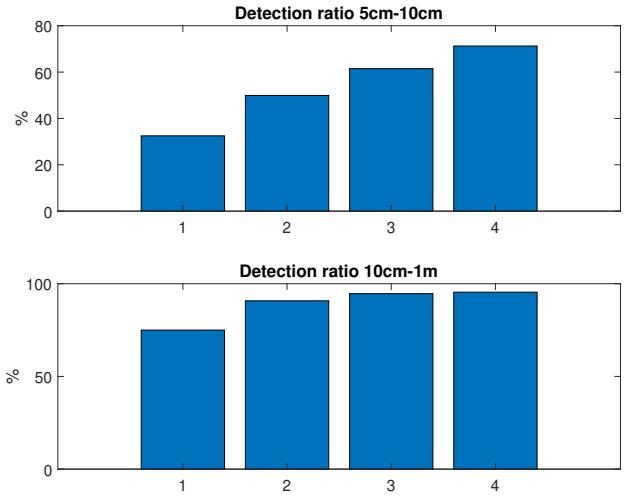

Figure 4.2: Detection ratio with debris dimensions for final four configurations

Regarding the configurations, the first architecture is simple and the instrument will be the actual size and form of the star sensor of the baseline.
Looking at the graph it is clear how the first instrument (configuration 5) is not capable of detecting the same amount of debris larger than 10 cm with respect to the other ones. It is important to underline how the other configuration, especially the last two, are capable of detecting almost 100 % of the debris. For this reason the first configuration is discarded.
The second and third configuration need a more complex design, the optimal solution instead of single sensors on the side of the satellite could be a unique body protruding out of the satellite with two or three optics pointed in the correct direction. This solution certainly reduces the size and encumbrance of the system, and it's considered better than having detached instrument in different points of the satellite.
The final configuration cant be built in a single block as the previous two and the best solution is having two separate blocks with two sensors each (like for the second configuration).
The next configuration to be eliminated is the one with 4 sensors, the extra ones do not lead to much higher detection rate. The major downside is having to mount two separate apparatus on opposite sides of the spacecraft, this leads to higher structural mass and much higher encumbrance having to reserve two separate slots for the instrument.
Regarding the choice between two or three sensors, it is is clear that these configurations can be mounted using the same frame. The only difference would be in the need of one extra optic and detector. Given the higher performances the configuration selected is the one having three separate sensors.

5 | Advance Design

5.1. Introduction

In this section the actual preliminary design of the instrument is initiated; this include an analysis on the instrument configuration, structure, optical components, electronics, OBDH and heat management system.
Once this phase of the design is done the actual capabilities of the instrument are obtained performing a simulation analysis and computing the the performances of the instrument. Below the design of each subsystem is reported below.

5.2. Detector

The detector is now accurately selected by searching for an existing component with the required characteristics, the major constraints are: 4096x4096 pixels, CCD technology and visible range sensitivity.
A first design choice regards the detector architecture and two main solutions are considered:

Full frame CCD,is the simplest form of sensor in which incoming photons fall on the full light sensitive sensor array. To readout the sensor, the accumulated charge must then be shifted vertically row by row into the serial output register and for each row the readout register must be shifted horizontally to readout each individual pixel. This is known as "Progressive Scan" readout.
A disadvantage of full frame is the incapability of measuring during the read-out process, the detection will happen during certain intervals of time.
A typical value for the read-out time is around 2 seconds for detector having 4096x4096 pixels.

Frame-transfer CCD uses a two-part sensor in which one-half of the parallel array is used as a storage region and it is protected from light by a light-tight mask.

Incoming photons are allowed to fall on the uncovered portion of the array and the accumulated charge is then rapidly shifted (in the order of milliseconds) into the masked storage region for charge transfer to the serial output register.
While the signal is being integrated on the light-sensitive portion of the sensor, the stored charge is read out. This means that the read-out and measurements are performed simultaneously, so the instrument can constantly detect. The major disadvantage is the size of this architecture, that is basically doubled with respect to the full frame CCD.

In this particular application it is fundamental to be able to constantly perform measurements in order to maximise the detection of space debris. One more advantage is that the final image reconstructed is going to show the entirety of the objects trajectory. For this reason the Full frame transfer technology is selected.

Once the basic detector architecture is selected, the main driver for selecting the component are small size, short read-out times, high Quantum efficiency and number of pixels. It is not possible to select an existing component for this function, since a frame transfer CCD detector with 4096x4096 acquisition pixels is not present in the market, for future development, the design and construction of this specific component is going to be needed. The general requirements for the detector are listed in Table 5.1, for specific parameters like: Input voltage, power consumption, and others, the values are based on similar existing detectors.

Parameter	**Value**
Number of pixels	4096x4096
Pixel size	9 $[m]$
Pixel case dimensions	36x72 $[mm]$
Total dimensions	50x100 $[mm]$
Read out noise	15 $[e/px/s]$
Full well capacity	10^5[e]
Read out rate	10 $[MHz]$
Quantum efficiency	0.6
Voltage supply	12 AC $[V]$
Power supply	0.4 $[W]$

Table 5.1: **Detector parameters and requirements**

5.3. Thermal system

5.3.1. Introduction

The instrument must be at certain temperature ranges in order to work correctly. The detector in particular must be constantly at low enough temperatures in order to limit the dark current noise and work properly. Temperature requirements are present also for other components of the instrument, as for example the processor, but they are less severe compared to the ones of the detector.
The design of the thermal system start with a general multi-node analysis on the instrument temperature ranges and subsequently of the detector. The first step is to compute the heat fluxes of the entire system

$$Q_{sun} + Q_{albedo} + Q_{irr} + Q_{sc} - Q_{ds} = 0 \tag{5.1}$$

Where:

- Q_{sun} is the heat due to the Sun radiation. The heat flux emitted by Sun is estimated as $W_{sun} = 1370 W/m^2$,
- Q_{albedo} is the heat due to the Earth reflected radiation, taken as 35% of the heat flux coming from the Sun, which is reflected by the Earth,
- Q_{irr} is the heat due to the Earth infrared emission. The heat flux emitted by Earth is estimated as $W_{irr} = 228 W/m^2$,
- Q_{sc} is the heat exchange by conduction with the spacecraft. The spacecraft is assumed at $283\,K$ in the hot case and $263\,K$ in the cold case,
- Q_{ds} is the heat exchanged by radiation with the deep space. The deep space is assumed at $4\,K$.

The next step is the modelling of the heat fluxes of the detector with the rest of the instrument and deep space.
It is considered that the detector exchange heat via thermal radiation with the detector box, in which it is contained and with the deep space (through the optical system). Regarding the heat flux given by the detector thermal dissipation, a cooling system will be adopted.

5.3.2. Radiator

The main focus of the thermal design is to keep the temperature of the instrument as low as possible (considering the boundaries of working temperatures of the components).
In order to reduce the Thermal radiation contribution coming from the Sun and Earth the entire instrument external area is covered with the *HiPeR laminate radiator* produced by *Airbus DS NL*. This laminate is a flexible foil consisting of one or more layers of Pyrolytic Graphite enclosed on both sides with a layer of Kapton, as shown in Figure 5.1.

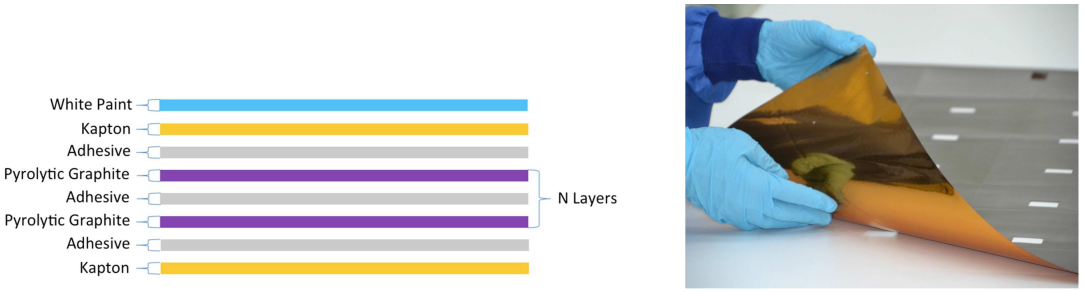

(a) HiPeR laminate. (b) Flexibility of the foil

Figure 5.1: Hyper Radiator

Finally, in Table 5.2 are reported the specifications of the radiator and the results obtained from its sizing.

Thermal Conductivity	Thickness	Area	Emissivity	Specific Mass
370 W/mK	0.3 mm	0.0445 m^2	0.9	0.56 kg/m^2

Table 5.2: HiPeR laminate data

5.3.3. Simulation and results

In order to evaluate the thermal behaviour of the system a *symulink* simulation is performed. During the passage of the satellite inside the Earth's shadow no heat contribution from Sun and Earth's reflection are considered. The analysis has the total time duration of 10 orbits in which the satellite and instrument switch between hot and cold case depending on the presence of Earth's shadow.
The modelled system has four nodes, one representing the instrument (including the detectors box) and the others the three detectors. The detectors will share the same temperature behaviour considering how the system has been modelled.

The heat radiation exchange between the detectors box (which are at the temperature of the instrument) and the detectors has been modelled considering average parameters for the emissivity of the surfaces and the thermal capacity. The heat exchange between the detector and deep space happen through the optical system of the instrument, an additional loss due to the lens presence is considered.

The results of the analysis for the temperature behaviour of both the instrument and the detectors are reported in Figure 5.2.

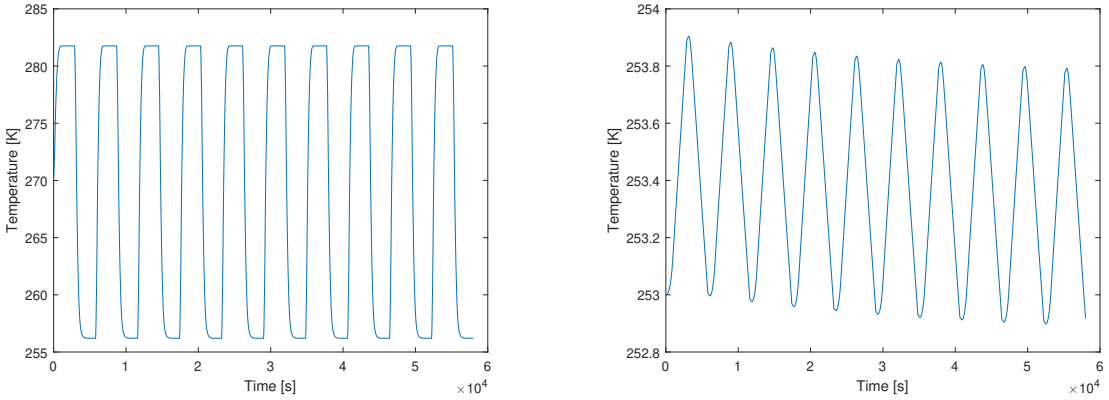

(a) Temperature evolution instrument. (b) Temperature evolution detector.

Figure 5.2: Systems temperature in 10 orbits

Analyzing the graphs, an oscillatory behaviour of the temperature is present since the satellite switches from hot case to cold case two times each orbit. The value for the maximum and minimum temperature for the instrument and detector are obtained. A maximum temperature for detector not exceeding 254 is ideal in order to limit the dark current noise and assure the proper functioning of the component.
As a last aspect of the thermal design, a system to control and dissipate the heat generated by the detector is designed.
The analysis is performed considering that the only input flux is the heat dissipated by the detector (0.4 W) and the only output flux is the one of the cooler. The cooler selected is an *OptoTECOTX* series, a miniature thermoelectric cooler capable of dissipating up to 1 W of heat. One for each detector need to be implemented and it has a total mass of 1 gram, dimensions of 1.6x0.1 mm and the required voltage supply is 2 V.

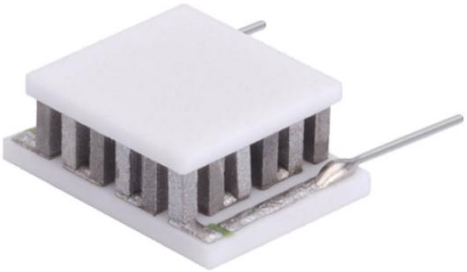

Figure 5.3: *OptoTECOTX* thermoelectric cooler

5.4. Optical system

The optical system is composed by these elements:

- Baffle
- Double-Gauss lens
- Filters

The **Baffle**, is an an opto-mechanical component present in order to limit the amount of straylight entering the system.

The **Double-Gauss lens**, consist of two back-to-back Gauss lenses(a design with a positive meniscus lens on the object side and a negative meniscus lens on the image side) making two positive meniscus lenses on the outside with two negative meniscus lenses inside them.
The symmetry of the system and the splitting of the optical power into many elements reduces the optical aberrations within the system. A quick sketch of this system is reported in Figure 5.4.

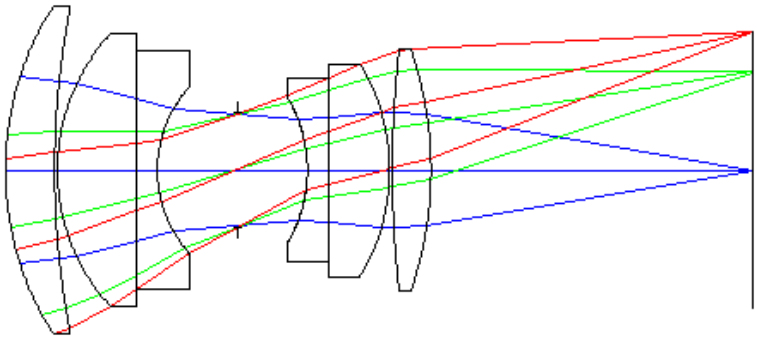

Figure 5.4: Double-Gauss lens

The **Filters** are components placed in front of the detector in order to limit the lights wavelength arriving. This is done since the detector is sensible to visible light only, light in other wavelengths would only increase the noise and temperature of the detector.

Regarding the optical system parameters, those are selected considering the instrument of the trade-off analysis and they are reported in Table 5.3. Changes in some parameters needed to be done since components like the detector, now that have been selected, have characteristics different with respect to the one of the preliminary analysis.

Parameter	**value**
Aperture diameter $[m]$	0.05
FOV $[deg]$	40
Detector dimensions $[m]$	0.0369
IFOV $[deg]$	$1.7044e^{-4}$
F number	1.0138
Focal length $[m]$	0.0507

Table 5.3: HiPeR laminate data

Regarding the singular lens, they are considered all made of the same material, glass $H-LAF1$, the mass of the system is estimated at 156 g, the value of optical transmittance is 0,8.

5.5. Power Distribution and Control Unit

The scheme representing the Power Distribution and Control Unit is reported in Figure 5.5. The power is assumed to come from the spacecraft main bus, the line is at 28 V and with a fully regulated bus voltage control. The full regulation is chosen because all the components of the instrument must be powered with their nominal voltage in order to work correctly. A bus switch is present in order to be able to turn off the instrument components at will, for example during the transit in Earths shadow where the instrument can not operate.

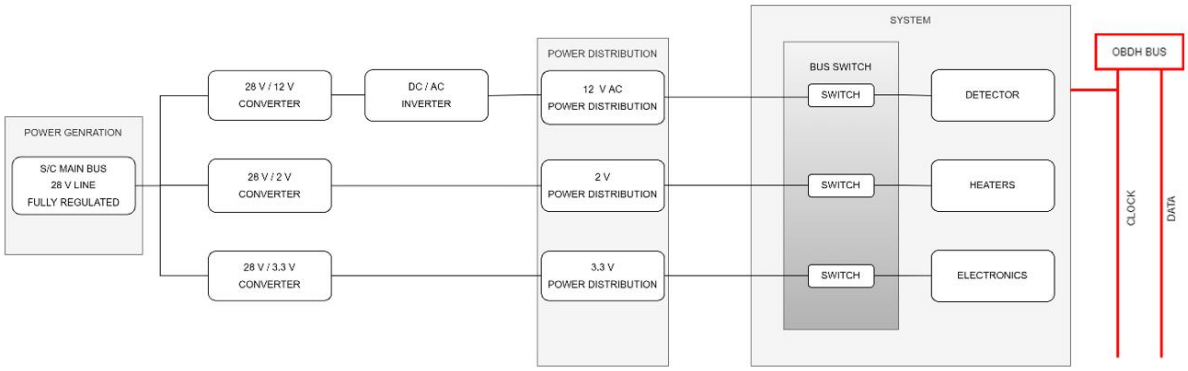

Figure 5.5: Power Distribution and Control Unit scheme

5.6. On Board Data Handling

This system has to link the spacecraft *OBDH* with the various subsystem of the instrument. The main processing operations are not done by this component and this includes the image processing of the acquired measurements.
The system must be able to gather the data from the three detectors and then handle it to the main computer of the spacecraft, at the same time the data must be momentarily stored in an memory. The memory must be capable of holding the information of a single analysis and it basically functions as a flash memory.
The *OBDH* system must also link the thermal and electrical subsystems with the main bus. The processing power for those activities is much less with respect to the previous one.

In order to design and size this component it is essential to understand the computing power required to perform the operations, the memory necessary to store data and the working frequencies necessary in order to function correctly with the other system com-

ponents.
The main performance requirements are related to the detector signal acquisition, as a first step the data flow and acquisition frequency for this component are studied.

The data from the detector is transmitted at a certain frequency, the system is going to sample and digitalize this signal, its frequency is equal to 10 MHz, the read out frequency of the detector. The sampling frequency obtained in order to respect the Shannons-Nyquist's theorem is set to 7 times the frequency of data acquisition and equal 70 MHz. Considering the detectors, it is a 4096x4096 pixel CCD frame transfer detector, the read-out time is around 1.7 seconds, the total number of pixels is 16.777.216. The data quantization selected is 8 bit, so for each pixels 8 bits are associated. From these values it is possible to compute the Mbit/s of data from a single detector as 78.5 Mbit/s, considering the presence of three detectors the total amount is 235 Mbit/s or 29.5 Mbyte/s.

In order to obtain the processing power required for all the system operations, an estimate on the needed $MIPS$ or Million Instructions Per Second is needed. This parameter is a general measure of computing performance.
The instrument processor must perform data acquisition and data processing and execution, each of these operations requires 2 instructions per pixels to be performed, so for each of the two operations a total of 19.6 MIPS is estimated.
Regarding the MIPS requirement for other processes, typical values are utilized.
In Table 5.4 it is reported an estimate of the total required $MIPS$, it can be seen how the amount for data acquisition and data processing and execution has been triple, since these operations are needed to be done for the data of each of the three sensors.

Type of instruction	Operations	MIPS required	Frequency
Data acquisition	2	59	70 [MHz]
Data processing and execution	2	59	70 [MHz]
Memory allocation	2	$2*10^{-6}$	1 Hz
Thermal control	-	$3*10^{-3}$	.
Power management	-	$5*10^{-3}$	.
TOTAL	-	118.011	.

Table 5.4: Instruction count

Starting from this data the Space grade RHBD processor LEON3, crafted by ESA, is selected. It has a medium cost while having good performance, radiation tolerance and it is capable of sustaining the MIPS required, the component characteristics are reported in Table 5.5. This processor is space grade, which means it can handle the harsh radiation environment and temperature of deep space. By encapsulating the processor inside a 4 mm thick aluminum sphere, the total radiation dose for the entire life-span is approximately 104, which is well-below the tolerance of the processor.

Production	2007
MIPS	150
TID tolerance	$300\,krad$
SEL	$> 118 MeV - cm^2/mg$
Temperature Range	$-55°C$ to $+125°C$
Data quantisation	32 bit core
Redundancy	Fault tolerance
I/O Voltage	$3.3\,V$
Max Clock	$125\,MHz$

Table 5.5: Instruction count

Now the system needs a flash memory in order to temporarily store the data of the acquisition, the memory selected must be capable of storing the data coming from the three detectors in one cycle, the safety margin selected is of 20 %, the total results for the memory requirements is 60 Mbytes.

5.7. Instrument configuration

In this section a general estimate on the power, mass and size budget for the instrument is presented. A basic sketch representing the instrument architecture and estimated size is reported in Figure 5.6.

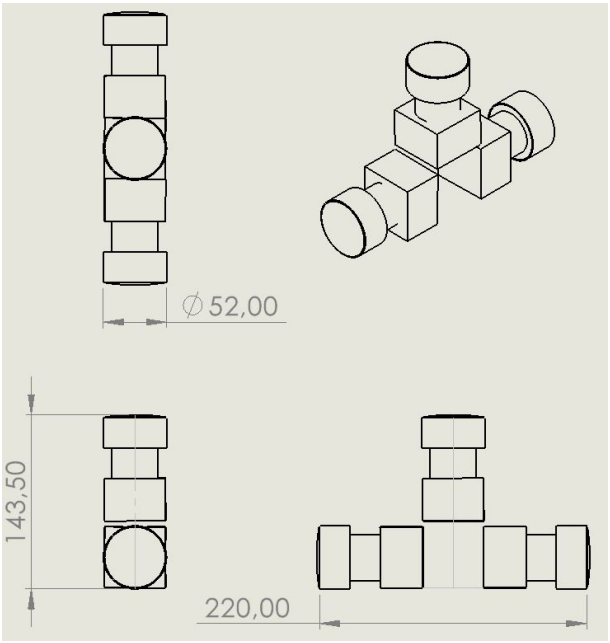

Figure 5.6: Instrument architecture

The estimation of mass and power of the instrument must take into account the maturity of the design and components. The general architecture of the system is based on existing star tracker and the components utilized are all flight proven; anyway the system is a new design and technology. For this reason the total mass and power margin is set to 25 %, the margin is applied also to single components or subsystems. This process is done accordingly to the AIAA standard for Conceptual Design Review stage.

The mass estimation of the system is reported in Table 5.6. It has been considered that some components, like detector and optics, are present in each of the three sensors.

Component	Mass (W/O margin) $[g]$	Margin	Mass $[g]$%
Detector	3x80	25 %	3x100
Optics	3x129	25 %	3x161
Sensor case	3x80	25 %	3x100
Electronic box	50	25 %	62.5
Exterior laminate	25	25 %	31.5
S/c interface structure	70	25 %	87.5
Supports and structural elements	200	25 %	250
Total w/o margin	1476	25 %	
Total	1845		

Table 5.6: Total mass estimation

The same procedure is done for the power requirements and reported in Table 5.7.

Component	Power (W/O margin) W	Margin	Power W%
Detector	3x0.4	20 %	3x0.5
Micro heater	3x0.4	20 %	3x0.5
Processor	9	20 %	10.8
Total w/o margin	13.8	20 %	
Total	16.56		

Table 5.7: Total mass estimation

5.8. Instrument performance

In this section the instrument is analyzed with the same metrics used in the previous trade-off analysis. This is done in order to estimate the general performances of the instrument.

Regarding the general capabilities of the instrument, a first study on the Range of the instrument with the debris size is performed, in Figure 5.7a the object diameter vary from 1 mm to 10 cm, while in Figure 5.7b from 10 cm to 1 m.

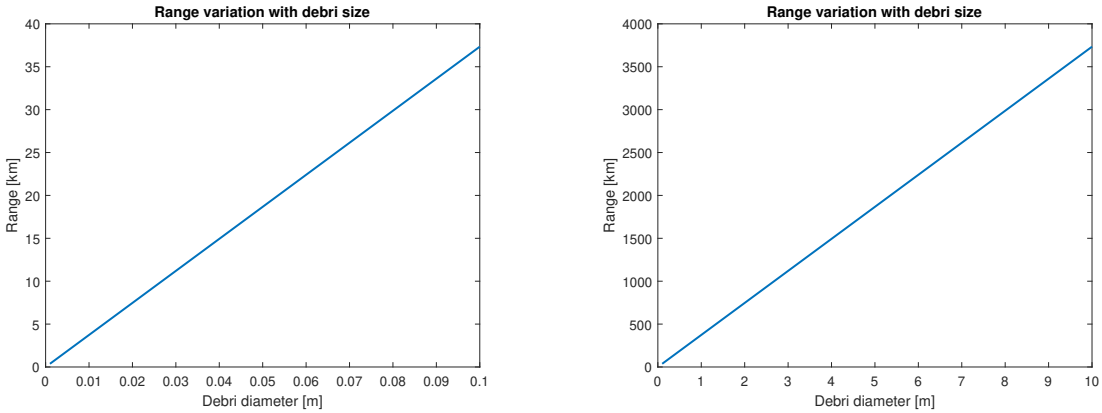

(a) Debris dimensions 1 mm to 10 cm.

(b) Debris dimensions 10 cm to 10 m.

Figure 5.7: Maximum range with debris diameter

As we can see the instrument still present a good maximum range while detecting small debris, as it will be shown in later analysis it could be a useful tool for the detection of debris under 1 cm too.
The minimum detectable magnitude of the instrument is 3.72, while the IFOV is $1.7044e-04°$. The next analysis regards the computation of the detection ratio of this final instrument. This study is done at first in the LEO environment (since the instrument design is based on LEO conditions), here the detection ratio is computed for debris size varying from 1 mm to 10 m. The instrument was designed trying to maximise the detection of only bigger debri (superior to 5 cm), but it is interesting to see the potential capabilities of the instrument in detecting smaller but still harmful debris.
The results for this analysis are reported in Figure 5.8, the general detection ratio of the instrument considering debris from 1 cm to 5 cm is 45, while for 5 cm to 10 m is 74.8 %.

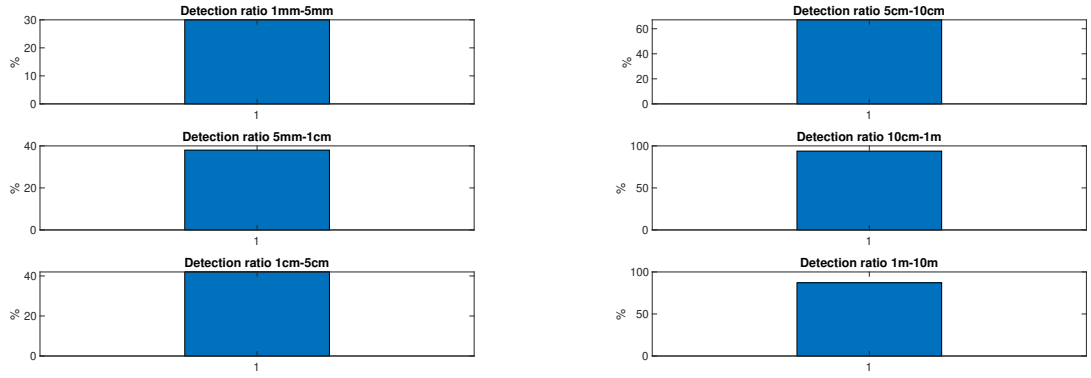

(a) Debris dimensions 1 mm to 5 cm.

(b) Debris dimensions 5 cm to 10 m.

Figure 5.8: Detection ratio with debris diameter

As it can be shown from the figure, debris with diameter larger than 10 *cm* are detected almost 100 % of the time, the detection ratio of very small debris, under 5 *cm* is significantly lower, but this does not represent a great problem since the main focus of the system is to detect larger debris.
It also has to be considered that the analysis was performed over a period of 10 days, over an higher time span the instrument could be capable of detecting an higher percentage of debris. This is not exactly true for all the cases since, especially for smaller debris, the orbit of these space objects varies rapidly in time so an analysis over a longer period of time could loose significance.
The same analysis is performed also in GEO orbits, as stated before this environment is of less importance with respect to the LEO one when talking about space debris; in fact the instrument was designed primarily to work in LEO. The analysis was performed over a period of 10 days and considering debris with dimensions superior to 5 *cm*, interestingly the result of the analysis show a detection ratio of 98 %, as it is also reported in Figure 5.9.

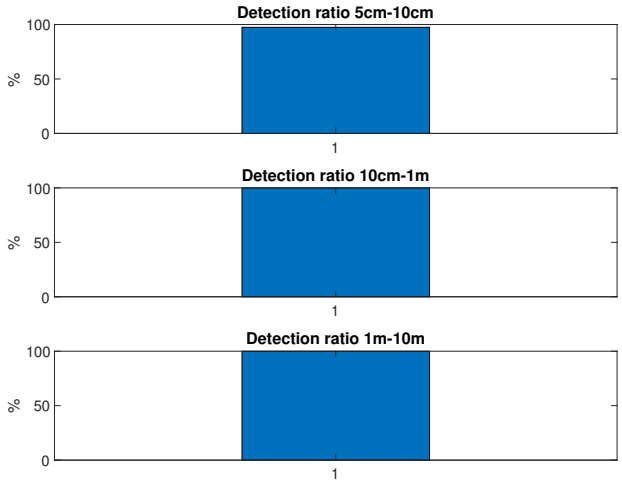

Figure 5.9: Detection ratio with debris dimensions

Here the performances of the instrument are much higher with respect to the LEO case, in fact high detection ratio values are present also for the smaller debris. There are two main reasons for this occurrence; the first one regard the debris orbits, as reported in Section 1.2.2 the typical orbital inclination is around 0 *deg*, with maximum and minimum of 15 *deg*, so there is a very small inclination difference with respect to the orbit of the satellite, meaning the detection and tracking of these object is going to be simpler.
The second reason is the much lower orbital velocities, these lead to debris passying by much more slowly and thus having more time for the detection. The debris will also stay inside a single pixel for a longer period of time, leading to a higher generated signal.

This mean that the instrument could be also be operated in the GEO environment, even if at the moment the problem of space debris is less relevant in that area.

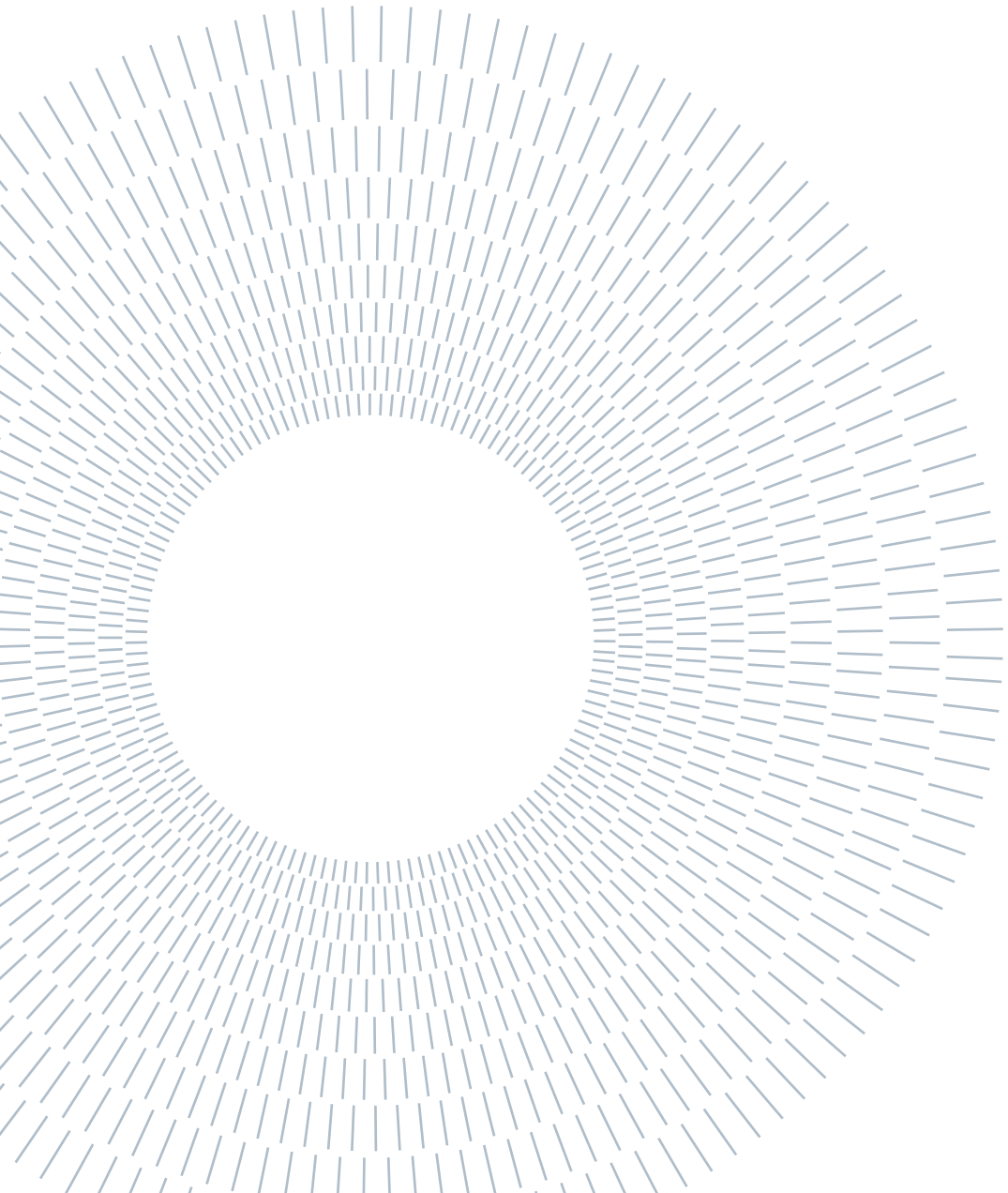

6 | Conclusions and future developments

In this thesis the initial design phases of an optical instrument for the detection of space debris have been discussed. The analysis is started from zero since there are no existing technologies similar to this one.
It was needed an extensive study on the debris environment to correctly define and understand the problem. Subsequently the design proceeded evaluating as much solutions as possible and selecting the most suitable ones. The thesis is concluded with an advanced design of the instrument, where subsystems and components are specifically designed and a more refined architecture of the instrument is obtained.
Anyway this does not mark the end of the development of the instrument. Much more iterations can be done in order to further optimize the design, a more specific design of the structure and configuration is needed in order to better estimate the mass and size requirements.
The system obtained at this point could potentially be an alternative to ground based sensors or an additional source of information to be integrated for better tracking and detection of space debris. The instrument does not present particularly high mass, power and size requirements and it could be a worth additional payloads in the bigger class of spacecrafts.

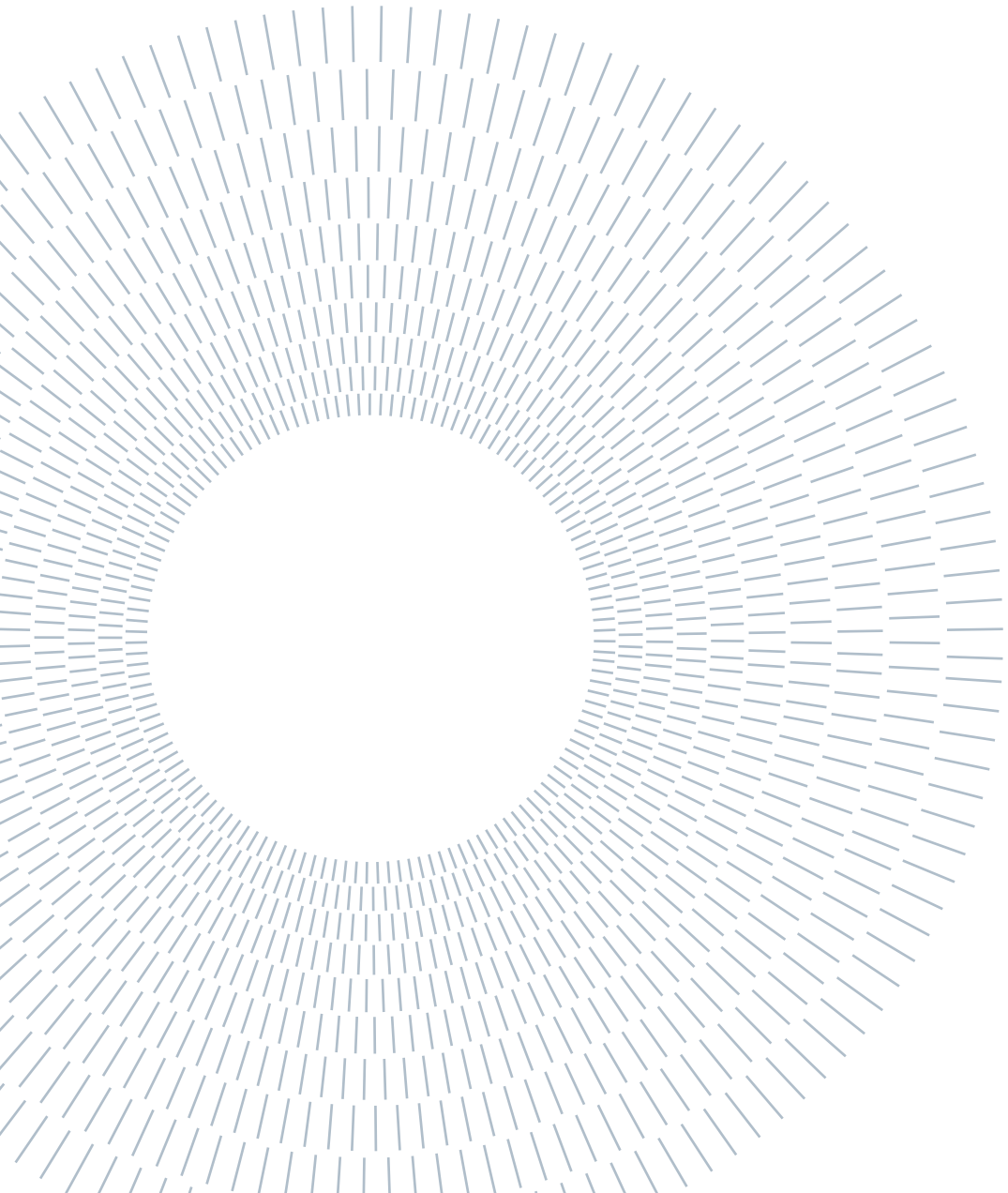

Bibliography

[1] Orbital debris: A technical assessment. *The National Academies Press*, page 22, 1995.

[2] P. Anz-Meador. Orbital debris quarterly news. *National Aeronautics and Space Administration NASA*, 2018.

[3] H. Cowardin, J. Hostetler, Murray, J. Reyes, and C. Cruz. Optical characterization of debrisat fragments in support of orbital debris environmental models. *The Journal of the Astronautical Sciences*, 2021.

[4] W. Dongfang, P. Baojun, and X. Weike. Geo space debris environment determination in the earth fixed coordinate system. *Hypervelocity Impact Research Center*.

[5] A. Horstmann, C. Kebschull, S. Müller, E. Gamper, S. Hesselbach, K. Soggeberg, M. Larbi, M. Becker, J. Lorenz, and E. Stoll. Survey of the current activities in the field of modeling the space debris environment. *Institute of Space Systems*, 2018.

[6] J. Shell. Optimizing orbital debris monitoring with optical telescopes. *US Air Force, Space Innovation and Development Center*.

[7] R. Thompson. A space debris primer. *The Aerospace Corporation*, pages 5–7, 2015.

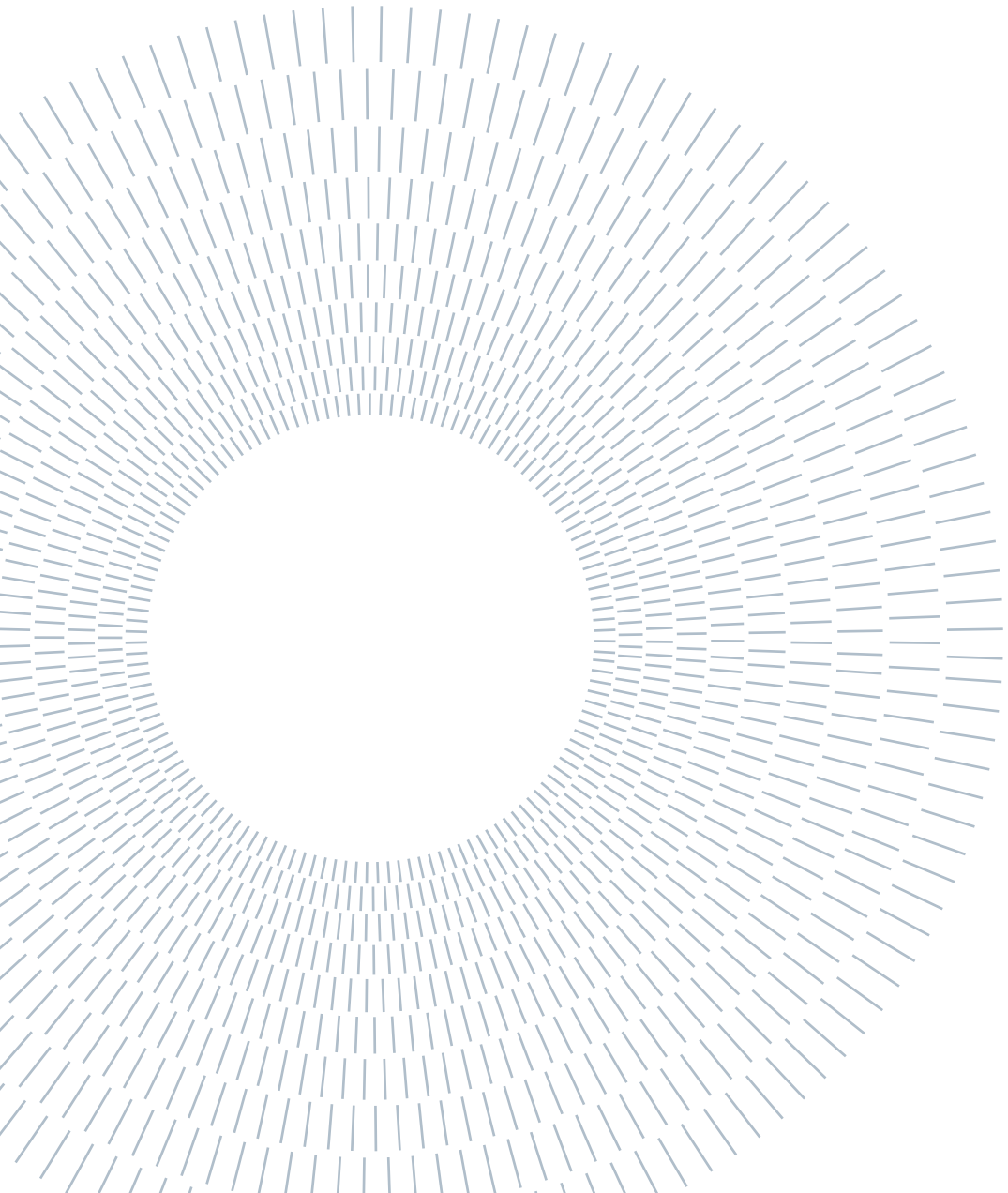

List of Figures

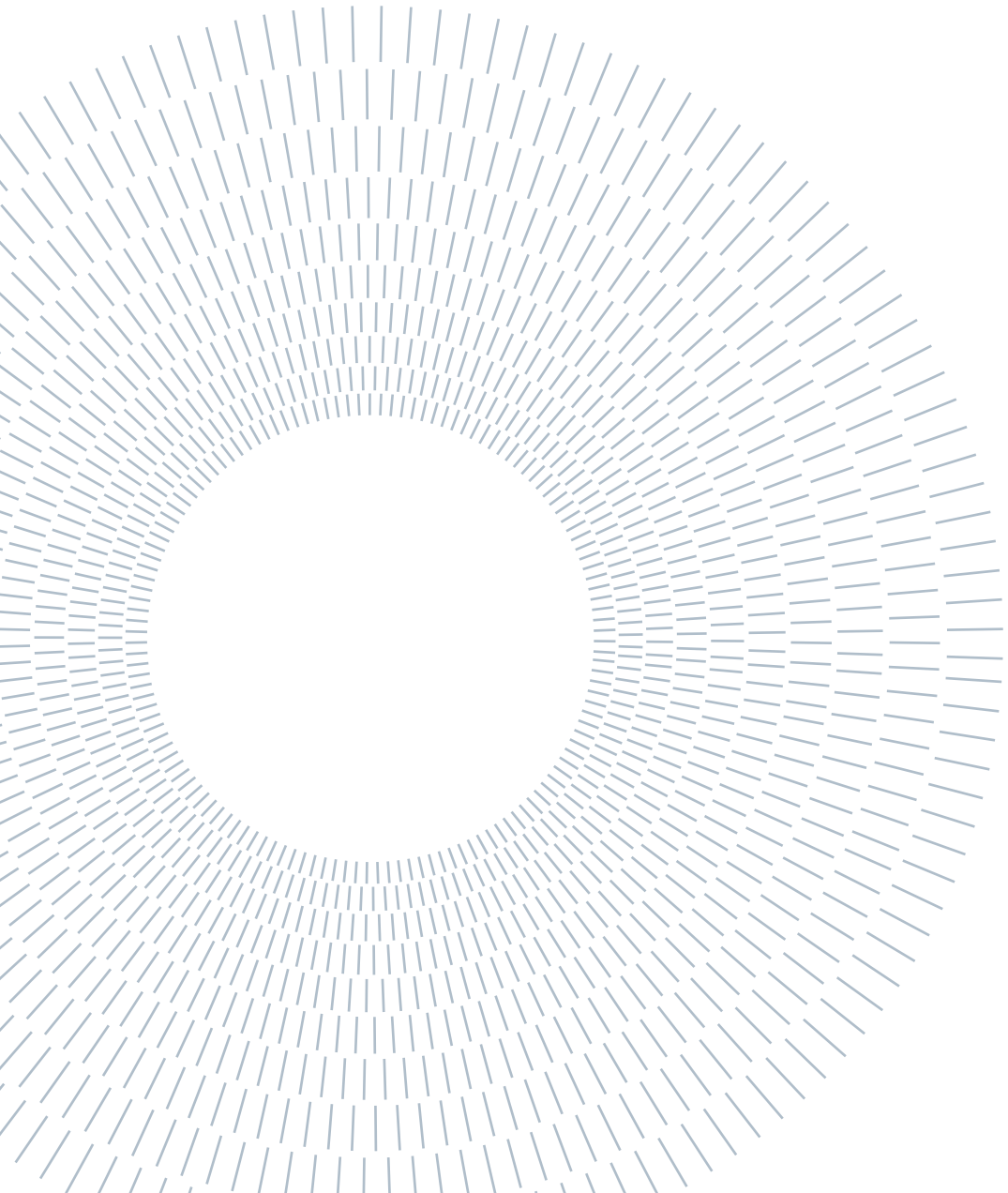

List of Tables

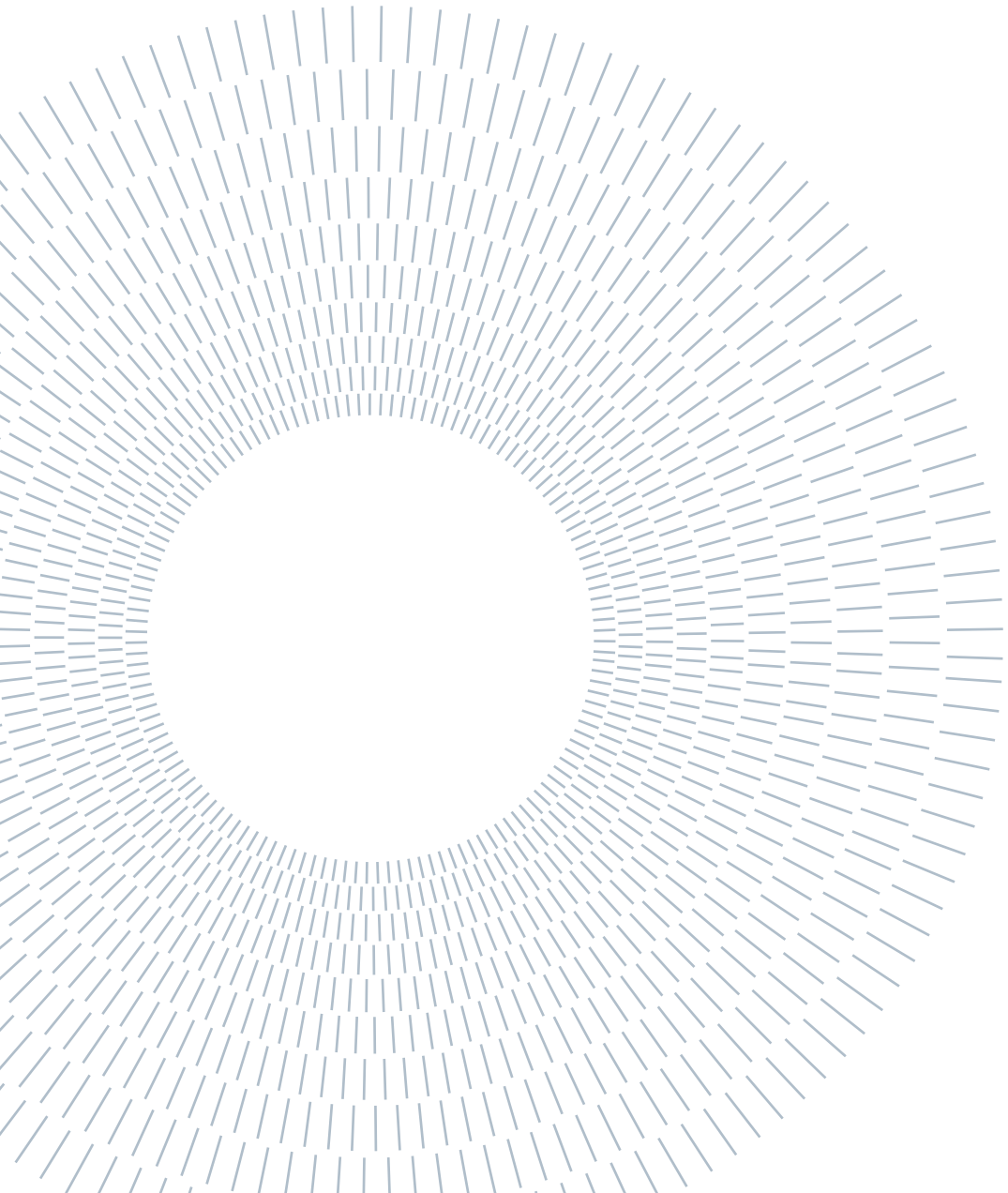

List of Symbols

Variable	Description	SI unit
SNR	Signal to noise ratio	-
e_s	signal photo electrons	$e^-/pixel$
e_b	Background noise photo electrons	$e^-/pixel$
e_n	Read out noise photo electrons	$e^-/pixel$
e_d	Dark current noise photo electrons	$e^-/pixel$
m_{obj}	Object visual magnitude	-
m_{sun}	Sun visual magnitude	-
d	Object diameter	m
ρ	Reflectance	-
ψ	Solar phase angle	deg
E_{deb}	Photon irradiance	$ph/s/m^2$
λ	Wavelength	m
h	Plank's constant	m^2kg/s
c	Speed of light	m/s
Q_E	Quantum efficiency	-
τ	Optical transmittance	-

Variable	Description	SI unit
A	Area	m^2
t	time	s
FOV	Field of view	deg
n_{pixel}	number of pixels	-
w	angular velocity	deg/s
L_b	Visual magnitude per square arc seconds	$ph/s/m^2/sr$
S_a	Solid angle	sr
G	Gain	-
d_s	Detector size	m
f	Focal length	m
F	F number	-
D	Aperture diameter	m
Q	Heat flux	W/m^2

Acknowledgements

I would like to thank my supervisor Mauro Massari, for his guidance throughout this project.
I am grateful for my parents whose constant support keep me motivated and confident. My accomplishments and success are because they believed in me.